CHAPTER 1
INTRODUCTION

1.1. Introduction

The worldwide increase in demand for the energy in the twenty first century has led to international cooperation to meet the energy needs without affecting the environment. The attention was drawn towards non-exhaustible and eco-friendly resources like tidal energy, solar energy and nuclear energy. This drive for alternative sources of energy brought drastic changes in the field of metallurgy; the limitation to increased efficiency is imposed by the metallurgical constraints. Renewable energy sources produce clean energy but it concerns about cost effectiveness and reliability. This led to the development of nuclear energy. The utilization of nuclear energy with proper care can reduce the dependence on fossil fuels. The structural materials for the nuclear power plants have to sustain consequences of radiation damage, disposal of radioactive waste after its service and effects of magnetic fields, etc. apart from high temperatures and accompanying thermal stresses.

International collaboration has suggested development of new reactors such as International Thermonuclear Experimental Reactor (ITER) [1], instead of depending on present generation of reactors. International Thermonuclear Experimental Reactor (ITER) is a collaborative venture proposed by several advanced countries to setup the world's largest tokamak. It is a magnetic fusion device capable of allowing fusion in large scale and generates carbon-free source of energy. The ITER demonstrates the integrated operation of technologies for a fusion power plant. This will bridge the gap between the present days smaller scale experimental fusion devices and with the fusion power plants of the future. This offers challenge to engineers and designers in selection of structural material. The ITER project includes studies on the development of fusion energy and assessment of various conceptual used in Test Blanket Modules (TBM) for tritium breeding. All the ITER participating countries (China, Europe, India, Japan, Korea, Russia and USA) are engaged in the TBM program for testing various types of tritium breeding modules. It is important that the alloy design for the structural materials incorporates necessary steps to reduce induced radioactivity and minimize the radioactivity level of the waste for safe disposal and storage.

Reduced activation ferritic-martensitic (RAFM) steels have gained attention as potential structural material for plasma facing blanket module in nuclear fusion reactors. These steels are specially developed in order to reduce the radioactive wastage after its service in fusion reactor application. The composition of RAFM steel is derived from the well-established modified 9Cr-1Mo steel by carefully substituting long half-life transmutant elements like Mo, Nb, Co, Al, Cu and N with elements having relatively short half-life transmutant elements like W, Ta, Mn and V. The steel possesses attractive properties such as high thermal conductivity, low thermal expansion coefficient, high resistance to radiation-induced void welling, helium embrittlement, and good compatibility with coolants such as lead-lithium liquid when compared with austenitic steels [2,3]. Conventionally, the RAFM steel is used in normalized and tempered condition, which consists of tempered martensitic microstructure. The tempered martensitic steel derives its high temperature strength from the complex microstructure consisting of high dislocation density; sub-grain boundaries decorated with chromium rich $M_{23}C_6$ carbides and MX type carbides/carbonitrides in the intragranular region. An important feature of this kind of steels is that the prior-austenite grain, packets, blocks and lath boundaries redistributes the stress induced by grain boundary sliding in such a way that usually no inter granular creep cavitation develops; rather the creep damage is in the form of microstructural instability manifested as reduction in dislocation density, coarsening of precipitates and sub-grain. However, unlike the MX precipitates, the $M_{23}C_6$ precipitates are prone to growth by Oswald ripening mechanism leading to the concurrent coarsening of martensitic lath substructures. The coarsening of $M_{23}C_6$ precipitates along with the replacement of MX precipitates with Z-phase particles have been reported to cause premature failure of long-term creep rupture strength of tempered ferritic-martensitic steels.

1.2. Background:

Until 1970's, the main candidate materials considered for fusion and fission power applications are austenitic stainless steels [4,5]. Soon, they were found unsuitable for fusion applications because of their high swelling tendency and induced thermal stresses owing to their high thermal expansion coefficient and low thermal conductivity. Despite this, they are still regarded as the worthy material for the construction of experimental reactors, viz. the International Thermonuclear Test Reactor (ITER). During the mid-1980s, ferritic/martensitic steels came in to

existence owing to their high resistance to swelling over austenitic stainless steels. Originally, the ferritic/martensitic steels were not explored neither for fission applications on account of high-temperature strength and coolant compatibility nor for fusion applications on account of the difficulties associated with the interaction of a ferromagnetic material in the high magnetic fields. 9-12% chromium martensitic steels with approximately 0.1–0.2% C, 1% Mo and small amounts of V, Nb, W, Ni, etc. possess the high-temperature strength and desirable thermal properties (high thermal conductivity and low coefficient of thermal expansion) that develop excellent resistance to thermal stresses [4]. In addition, these steels exhibited good creep strength up to 550 to 600°C. As a result, these steels are considered as good candidate materials for use in the power-generation and chemical and petrochemical sectors at these temperatures. For higher operating temperatures of fusion plant (≥700°C), special materials such as refractory metal (Nb, Mo, V, and Ti) alloys and super alloys were considered.

Currently, the three candidate materials considered for the construction of fusion power plant components are: vanadium alloys, SiC/SiC composites, and ferritic/martensitic steels [6]. Among these, ferritic steels are considered to be advantageous for fusion power plant as they are capable of fabricating in to massive structures. In case of vanadium and SiC/SiC composites, the methods for fabricating massive structures (joining, etc.) are yet to be explored. Further, these materials are prone to many other problems which are to be resolved prior to their successful use. Earlier research shows that many of the refractory metal alloys have been avoided for the construction of first wall and test blanket modules owing to lack of physical or mechanical properties or fail to meet the reduced-activation criterion.

High-chromium ferritic/martensitic steels are considered mainly in the fuel subassembly as fuel pin cladding and wrapper material. However, the utilization of these steels for the construction of first wall and test blanket module of a fusion plant possess a big challenge. This necessitates focused research for the determination of required properties for this application. The maximum operating temperature of these steels will be decided by their creep properties and found to be potential materials up to 550 to 600°C for fusion applications.

1.3. Low- and Reduced-Activation considerations

Despite possessing high elevated temperature strength and oxidation resistance, high resistance to swelling, high thermal conductivity and low thermal expansion coefficient, another important characteristic of structural materials used for fusion power plant is 'low-activation'. Low-activation refers to mild or nil radio activity. Therefore, a 'low-activation' material is the one that satisfies any one of the following criterion: (i) it would not become radioactive; (ii) it would activate to a low level prescribed by environmental standards; (iii) if activated, it would rapidly degrade (within minutes or hours) to a low level after activation during normal operation as well as accident conditions [7]. In other words, a low-activation material would eliminate the adverse effects caused by an unexpected exposure of radioactive debris. Such a material would also permit easy maintenance of the plant without complex and expensive remote maintenance. Therefore, it is utmost important to consider the environmental safety when fusion structures are fabricated from a vanadium alloy, a SiC/SiC composite, or reduced-activation ferritic steel [6,8] . Until now, ‘low-activation’ materials specified as above does not exist. A recent study [9] in the European Union shows that the activation of SiC, developed for ‘reduced activation’, is notably lower than a V-5Cr-5Ti alloy and a Cr-W ferritic/martensitic steel (OPTIFER). However, they do not meet up with the criterion of low activation as explained above.

When the fusion reactor components with induced radio activity are replaced during operation or decommissioning of the old nuclear power stations, a considerable amount of radioactive waste is generated, which is to be disposed in a safe manner without creating any environmental effects [7]. Depending on the alloying elements present in traditional ferritic/martensitic steels, it can take thousands of years for the decay of induced radioactivity. A deep geological storage is required to dispose such a highly radioactive waste. To address this issue, research programs on the development of ‘low-activation’ or ‘reduced-activation’ ferritic steels were started in the Europe, the Soviet Union, the USA and Japan [10–16] with a primary objective of recycle of the material or shallow land burial after its service period without adverse environment effects. These new ‘reduced-activation’ ferritic/martensitic steels exhibit the similar behaviour as with the traditional steels with minor differences.

Based on the above information, the steels for fusion applications should contain only those elements that do not form radioactive products; or if formed, they should decay quickly to low

levels in short durations, say tens or hundreds of years rather than thousands of years. Calculations [10] shows that the alloying elements with long-life radio activity, such as Mo, Nb, Ni, Cu and N in Cr-Mo steels must be substituted by those elements which produce short-lived radioactive products. With this concept, the reduced-activation ferritic steels [9,10,19,11–18] were evolved. In these steels, molybdenum is substituted by tungsten and/or vanadium and niobium by tantalum in conventional Cr-Mo steels. Final radioactivity levels in such 'reduced-activation' or 'low-activation' steel is found to be much lower than in conventional Cr-Mo steels. Such steels can be either recycled or disposed by shallow land burial, thereby a significant economic benefit can be obtained. Consequently, the steels for fusion applications are designed and developed without the addition of restricted elements like Mo, Nb, Ni, Cu and N. Their mechanical and physical properties were evaluated and found to be good or better than traditional Cr-Mo steels [9,12–14,16–19]. Apart from the above said restricted elements, it is required to restrict other elements such as Co, Bi, Cd, Ag, etc. to extremely low levels to meet the objective of recycling or shallow land burial after their use [20,21].

1.4. Problem identification and motivation of the work:

Many of the traditional Cr-Mo steels are in use for high-temperature applications in the temperature range of 550 to 600°C in petrochemical and power-generation sectors. Extensive research on traditional Cr-Mo steels resulted in well documentation of the metallurgical characteristics and physical and mechanical properties and hence comprehensive mechanical property compilations are available. However, substantial data is not available on reduced-activation steels either in the irradiated or unirradiated condition as extensively available for the traditional Cr-Mo steels.

At present, most of the research on RAFM steels is focused on the evaluation and use of the steel in normalized and tempered heat treatment condition and the adjustment of chemical composition for improving the specific mechanical properties. Efforts are in progress to increase the microstructural stability of the steel by micro alloying with boron, cobalt, copper and control on nitrogen content [22,23]**.** Thermomechanical treatment (TMT) of the steel is another area, which is not explored fully, and which has high potential in enhancing the high-temperature properties of the steel without any change in chemical composition [24]. The dislocation substructures produced on TMT process is expected to facilitate refinement of lath structure, and

precipitation of numerous numbers of $M_{23}C_6$, and MX carbonitrides by providing nucleation sites thus leading to enhancement of properties. A study carried out on modified 9Cr-1Mo steel [25] showed enhanced precipitation of nano-sized MX type precipitates over $M_{23}C_6$ on TMT processing, thus increasing the resistance to creep deformation and rupture life**.** However, a few/very limited research has been carried out using TMT for the improvement of creep rupture life of RAFM steel. In the present investigation, it is intended to improve creep strength of RAFM steel by the modification of quantity, size and morphology of $M_{23}C_6$ and MX type precipitates through TMT.

The extensive literature survey on RAFM steels describes the efforts made over the years by several researchers to improve the microstructural stability and strength properties.

(1) Use of TMT and designing the appropriate TMT cycle to improve the microstructural stability and texture hardening of RAFM steel. TMT is not explored fully in the evaluation of RAFM steels.
(2) Determination of high temperature properties (tensile and creep) of RAFM steel in TMT condition and to envisage the reasons for failure by pre- and post-tensile microstructural investigation is not documented.
(3) Identification of the perfect constitutive flow equation of RAFM steel in TMT condition and to correlate the experimental strength parameters with the analytical parameters is not studied.

1.5. Objectives of the present study

1. To study the effect of TMT on microstructure, hardness, tensile properties, flow and work hardening behaviour, RAFM steel and compare with those in normalized and tempered condition.

CHAPTER 2
LITERATURE SURVEY

2.1. International thermoelectric reactor (ITER)

Nuclear fusion is a process wherein nuclei of low atomic numbers combine and form heavier nucleus with the release of neutron and massive energy. Equation 2.1 shows the basic fusion reaction that occurs between deuterium (D) and tritium (T), the two isotopes of hydrogen.

$$^{2}D_{1} + {}^{3}T_{1} \rightarrow {}^{4}He_{2}\ (3.5\ MeV) + {}^{1}n_{0}\ (14.1\ MeV) \qquad (2.1)$$

The deuterium (D) and tritium (T) combine together and release a helium nucleus and a neutron with energies of 3.5 MeV and 14.1 MeV respectively. The total energy released is shared in the ratio of 20:80 by the helium and neutron.

The schematic diagram of the experimental nuclear fusion power plant is shown in **Fig.2.1**. Deuterium is readily available as it present naturally in water; whereas tritium has to be generated *in situ* as it is not naturally available. Tritium is generated by interaction of the neutron, a product of fusion reaction, with lithium (as shown in **Fig.2.2**) in lithium blanket in the reaction chamber **(Fig.2.1)**. Therefore, the fundamental fuels for fusion are lithium and water which are readily available. Most of the energy is released as heat and used to generate steam which drive turbines and hence produce electricity as in conventional power plants.

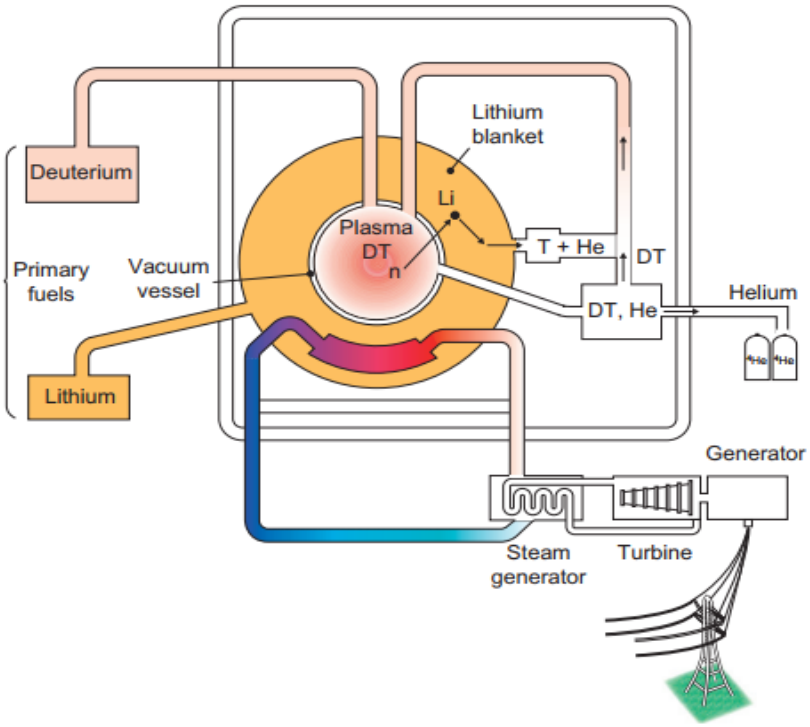

Fig.2.1. Schematic representation of nuclear fusion power plant [26]

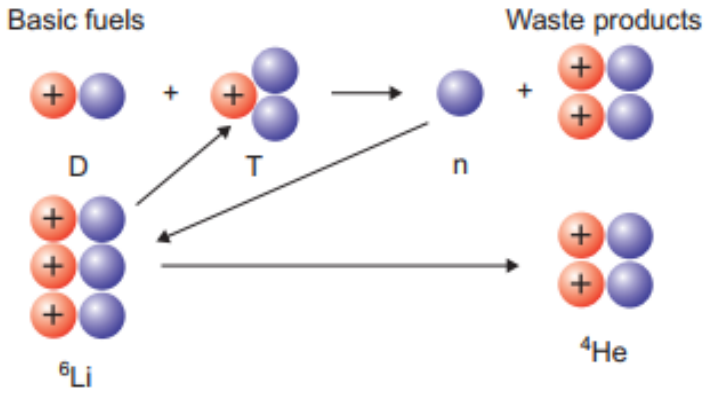

Fig.2.2. Illustration of tritium production in situ in a power plant [26].

Plasma is the fourth phase of matter and at extreme temperatures electrons are separated from nuclei and produce mixture of nuclei and electrons. In ITER, fusion process is achieved in a vessel called tokamak (**Fig.2.3a**) that uses magnetic field to control the shape of the plasma. The heart of the tokamak is doughnut-shaped vacuum chamber. Two types of magnetic fields are maintained in tokamak i.e. toroidal field and poloidal field (**Fig.2.3b**). Both the magnetic fields combine and create a composite magnetic field that causes doughnut-shaped plasma (**Fig.2.3d**). As the neutron has no electric charge, it is not affected by the magnetic field. It escapes from the plasma, hit the surrounding structure (blanket modules **Fig.2.3c**), transfers its energy and combines with lithium in lithium blanket to produce tritium. The helium with some amount of heat energy is confined by the magnetic field and is used to heat the plasma. In the beginning, an external source of energy is used to heat the gas or raise the plasma temperature. In the later stages, this heat is enough for continuing the fusion reaction.

2.2. Material requirements for fusion reactors:

The major components of ITER are the plasma facing components namely the first wall and breeding blankets, which are exposed to high neutron irradiation, higher mechanical, thermal, and electromagnetic loadings under static and transient conditions [27,28]**.** The selection of material requirement for the fusion reactor application is considerably more difficult than the conventional energy systems due to safety and regularity concerns [29,30] and availability at optimum overall material life cycle cost. The selected material should possesses attractive properties such as high thermal conductivity, low thermal expansion coefficient, high resistance to radiation-induced swelling [31] and helium embrittlement [32,33], and good compatibility with coolants such as lead-lithium liquid [28,34,35] , high temperature strength under neutron irradiation [30,36], and more importantly low activation under service condition. The fusion reactor system consists of (i) burning plasma (ii) plasma support system includes (magnets, plasma heating and current drive, plasma fueling), (iii) fusion nuclear core and balance of plant [37]. The fusion nuclear core or plasma chamber consists of first wall blanket, divertor, elements of plasma heating, fuelling and vacuum pumping ducts, radiation shields and vacuum vessel. **Figure 2.4** is the artistic schematic view of material layout around the plasma in tokamak.

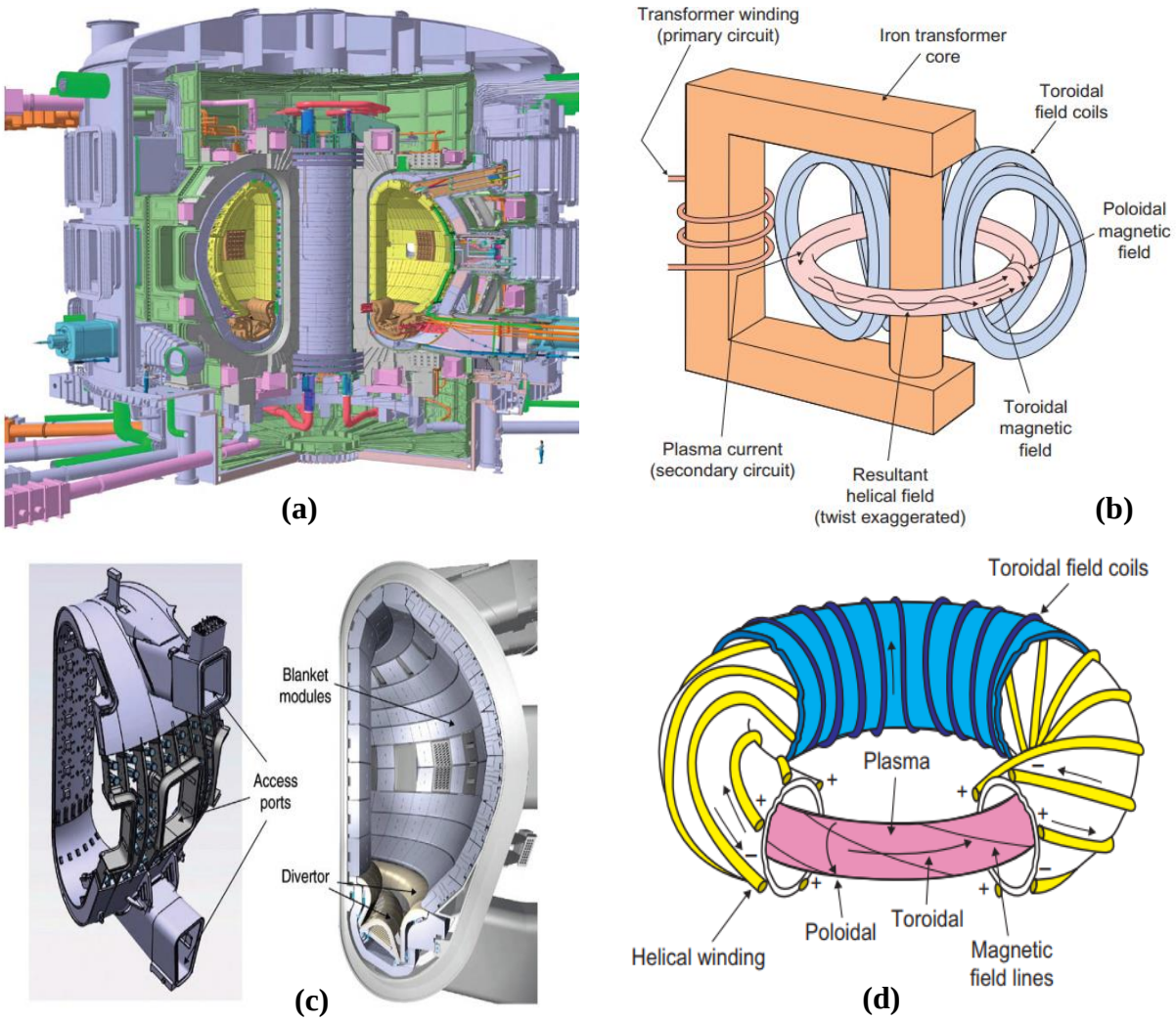

Fig.2.3. Various parts of International thermoelectric reactor **(a)** Cutaway model of tokamak, **(b)** Magnetic confinement **(c)** Test Blanket modules and **(d)** Doughnut-shaped plasma [26]

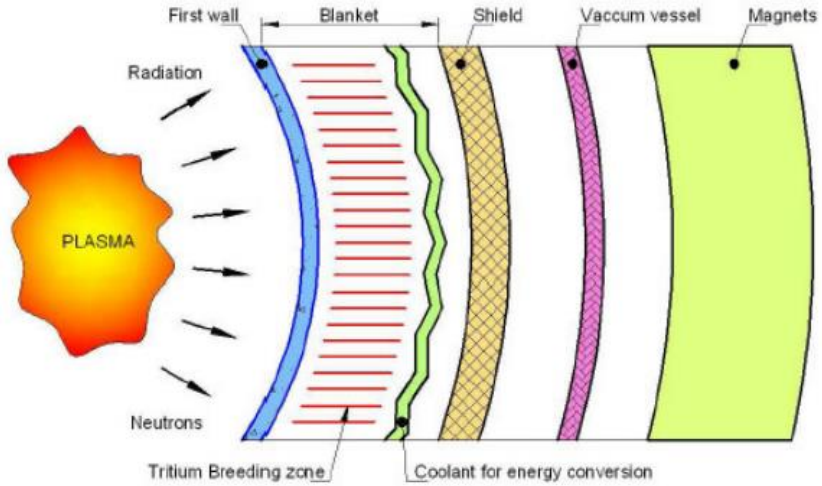

Fig.2.4. Schematic view of the arrangement of materials in a tokamak [37].

The blanket is an important component in the fusion reactor, which directly faces the plasma radiation and it extracts heat from it and also acts as a tritium breeding to ensure tritium self-sufficiency. The first wall of the tokamak is the one which directly faces of plasma and it experiences higher He/dpa ratios due to damage owing to high heat flux and high energy neutrons. Similarly, the divertor also falls under the same category. To avoid this, an element is chosen such that it does not sputter due to hitting of neutrons or, else, does not quench the plasma despite the fact that sputters is selected. Based on this knowledge low atomic number Be, C-C-composites are chosen even though they generates high sputters but having less plasma quenching feature, or else high atomic number based alloys of W and Mo are chosen which having low sputtering nature although it consists of high plasma quenching feature [6,37].

In general, low activation ferritic-martenisitic steels, JLF-1, F82H, EUROFER97 or their equivalent steels are chosen as first wall structural material due to their low swelling under irradiation [38,39]. The steel is alloyed with chromium, tungsten, vanadium, niobium, tantalum, carbon, nitrogen etc. to have complete hardenability (100 % martensite) with no traces of ferrite on air cooling from austenitization temperature, and intergranular $M_{23}C_6$ and intragranular MX precipitates on subsequent tempering. Molybdenum and niobium in these steels are replaced by tungsten and tantalum respectively to make the steel as RAFM with much reduced residual radioactivity on neutron exposure [40].

The tritium breeding blanket Li^6 is in the form of ceramic compound or liquid metal is selected [37]. The Li^6 transmutes to tritium after reacting with the 14.1 MeV neutrons which is escaped from the doughnut shaped plasma during fusion process, it also heats up the structural material. This reaction also leads to the formation of both hydrogen and He at higher rates. The shape of the plasma was confined by using super conducting magnetic fields i.e. torodial and polodial type and it confines the plasma into doughnut shape kind of ring in the vacuum vessel [26]. Generally, Nb_3Sn superconducting material was used as magnets to create the field and control the plasma shape [26,37]. The stainless steel cryostat surrounds the super conducting magnets and the vacuum vessel provides ultra-cooling to the system and also vacuum environment. The divertor acts as a heat sink, positioned at the bottom of the vacuum vessel, it controls the exhaust of waste gas and impurities, carries away the heat and avoids excessive heating. It withstands to the excessive loads in the reactor. Divertor is generally fabricated with alloys of Cu-Cr-Zr or Cu based alloy-dispersion strengthened by alumina [37].

2.2.1. 9Cr-1Mo steels

These steels have been classified as **(a)** unmodified and **(b)** modified based on alloying addition. The unmodified steels contain typically 9-12%Cr, 0.1-0.2% carbon and 1%Mo (P9/T9). Modification is achieved by the addition of carbide forming elements such as V, Nb along with controlled N which has resulted in the Grade 91 or the Mod P91/T91 steels [1,40]**.** The composition of these steels is presented in **Table 2.1**.

(a) Plain or unmodified 9Cr-1Mo steels (T9/P9):

9-12 % Cr-1%Mo steels have high resistance to oxidation at elevated temperatures (<538°C) and favourable thermal properties like high conductivity and low expansion coefficient. Plain or unmodified steels comes under zeroth generation (years 1940-60) of ferritic-martensitic steels in power generation industry and are in use to operate at maximum temperature of 520-538°C and stress levels below 40 MPa (10^5 rupture strength, 600°C) [1,40].

(b) Modified 9Cr-1Mo steels (T91/P91 or Grade 91 steel)

The modified 9Cr-1Mo ferritic steel is an improved version of plain 9Cr-1Mo steels and is widely used in thermal power plants for the steam generator applications. This steel comes under second generation (years 1970-85) of ferritic-martensitic steels in power generation industry. The steel is generally used to operate at maximum temperature of 593°C and stress levels of 100 MPa (10^5 rupture strength, 600°C) [1,40]. The steel is best used in fossil fired thermal industry due to its low thermal expansion coefficient, resistance to corrosion compared to austenitic steels and high mechanical properties including low cycle fatigue, tensile and creep at elevated temperatures.

In order to further improve the power plant operating temperatures and stress levels, the steel is modified by the addition of boron (B) by controlling the nitrogen (N) to avoid the formation of boron nitride (BN). This steel exhibits higher creep rupture properties [40–43].

Table 2.1 Chemical composition of 9Cr-1Mo and Mod 9Cr-1Mo steels (wt. %) [40]

Steel	C	Si	Mn	Cr	Mo	V	Nb	N	Fe
9Cr-1Mo (T9)	0.12	0.6	0.45	9.0	1.0	—	—	—	Balance
Mod 9Cr-1Mo (T91)	0.10	0.4	0.40	9.0	1.0	0.2	0.08	0.05	Balance

2.3. Development of low/reduced-activation ferritic-martensitic steels for nuclear reactors:

The structural materials used in the nuclear reactors are required to withstand high temperature thermal stresses, damage due to radiation and high magnetic fields. The austenitic stainless steels are considered as first option for fission and fusion power plant applications [1,44,45]. But, the major issue with these austenitic stainless steels is their high swelling tendency and structural distortion [31,46]. Materials such as Si/SiC composites [8], vanadium alloys [6,8], oxide dispersion strengthened (ODS) alloys [46–48] and ferritic/martensitic steels [8,29,49,50] are identified for use as structural materials in fusion reactors. The first two materials pose unresolved issues related to their fabrication. Although, oxide dispersion strengthened (ODS) alloys having ferritic matrix and dispersion of yttria and titania have been developed [51], their anisotropy is the major setback. The experience from fast reactors has demonstrated that ferritic/martensitic steels showed higher resistance to irradiation induced void swelling, better thermal conductivity, greater resistance to oxidation at elevated temperatures, high creep resistance and excellent room temperature ductility and toughness [46,49] which makes them a natural choice as structural material for the test blanket module (TBM)**.** Therefore, ferritic-martensitic steels have become suitable choice to use as structural materials in fusion reactors. The ability of a material to be used for structural applications shall also fulfil requirements such as availability, economy, and ease of field-erection. The choice of ferritic/martensitic steel is also aided by its technological maturity with respect to industrial production, fabrication and testing methodologies [37,52,53]**.** In addition to the aforesaid requirements, the material should also possess ‘low-activation’ property. It means, in radioactive environment, when irradiated the material do not become radioactive or if activated, the radioactivity should decays quickly. This low activation feature provides necessary protection from radioactive debris in extreme case of

accidental situation and also permits easy disposal of radioactive waste. Therefore, it is necessary to develop and use low-activation steels.

The modified 9Cr-1Mo steel do not satisfies the term low-activation since the alloying elements such as Mo and Nb present in it transmute on neutron irradiation and produce long lived isotopes. No structural material was developed so far to meet the criterion of 'low-activation' discussed in chapter 1, section 1.3. Efforts are continuing internationally to produce 'reduced-activation' steels. These steels can be disposed easily by shallow land burial or recycled after adequate cooling period of about 100 years. The practical limitation imposed by industry and economic considerations for achieving "low-activation" has enabled the development of reduced-activation ferritic-martensitic (RAFM) steels [1,38]. It is important that the alloy design for the structural materials incorporates necessary steps to reduce induced radioactivity and minimize the radioactivity level of the waste for safe disposal and storage [11,19]. The calculated radioactivity of few alloying elements of steel, on exposure to typical fusion neutron spectrum is shown in **Fig.2.5**. The alloying elements such as Mo, Ni and Nb need to be eliminated to obtain low level of radiation after about 100 years of cooling time. In this context, the composition of the modified 9Cr-1Mo steel has been tailored by replacing long half-life transmutants Mo and Nb with comparatively lower activation counterparts W and Ta respectively to make the steel as reduced activation. Besides these, it is also necessary to restrict the other residual elements such as Co, Bi, Cd, Ag, O, Ni, etc. of the steel to have a low induced radioactivity in the material and thereby to simplify the need of special requirements for the maintenance of fusion reactors after their shutdown [54,55].

Efforts are made by various countries notably European Union, USA, China, Japan and India to optimize the chemical composition and heat treatment of RAFM steel. Many countries developed RAFM steels by taking the reference of EUROFER 97 [6,56–59] for meeting the requirement of ITER-TBM.

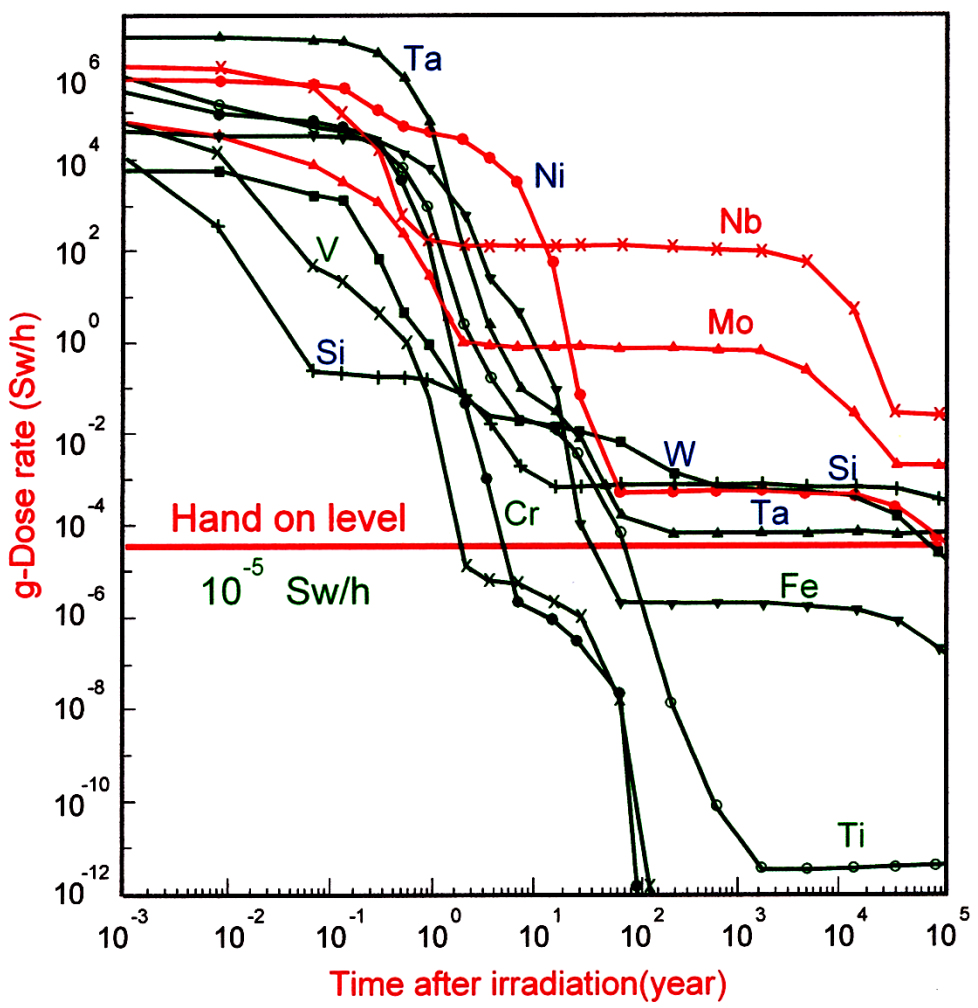

Fig.2.5. Calculated radioactivity on few elements versus time after exposure with respect to typical fusion neutron spectrum [54].

2.4. Design of RAFM steel

The development of RAFM steel follows the below guiding principles:

(i) Replacement of radioactive undesirable elements such as molybdenum, niobium and nickel from the existing modified 9Cr-1Mo ferritic martensitic steels by elements such as tungsten, vanadium and tantalum which have equivalent or similar effects on the constitution and structure but less prone to induced radioactivity upon prolonged neutron irradiation.

(ii) Removal of impurities like B, Cu, Ni, Al, Co and Ti, which are prone to transmutation on neutron irradiation.

(iii) Strict control on tramp elements such as S, P, As, Sb, Sn, Zr and O which promote embrittlement [53,65]**.**

Several variants of RAFM steels have been developed in various countries like F82H, JLF-1 (in Japan), Eurofer97 (in Europe), ORNL-9Cr2WVTa (in US) and INRAFM (in India) and extensive research is underway [6,49,56–63]**.** The compositions of the RAFM steels are already presented. Besides meeting the nuclear properties such as good resistance to void swelling, helium embrittlement, and mechanical properties, 9Cr RAFM steels have good thermal conductivity, low thermal expansion coefficient and good compatibility with wide range of liquid and gaseous coolants.

2.5. Alloying elements of RAFM steel:

Carbon (C) is an important alloying element out of all. It dictates the hardness and impact strength of the steel. The amount of C content has great influence on parameters like M_s and M_f temperatures, hardenability, amount and type of precipitates formed. This element was a strong austenite stabilizer with a relatively large solubility in austenite and having less solubility in ferrite which gives rise to the formation of carbides [1,66].

Chromium (Cr) is another important alloying element in RAFM steel. It is a ferrite stabilizer and strong carbide former. It is added to the steel to offer high oxidation and corrosion resistance. This element forms the precipitates of the form $M_{23}C_6$ (where M = Cr, Fe and W; but, mostly Cr rich). Addition of higher amount of Cr to steel is limited to avoid formation of delta ferrite which is known to have detrimental effect on elevated temperature properties. The optimum Cr content

is considered as 9% on the basis of (i) the longest creep life and (ii) lowest increase in DBTT on irradiation [17,38,49]**.** Addition of higher Cr content also assists in the accelerated formation of Z phase that takes up other elements like V, Nb and N from the matrix [67].

Tungsten (W) is a strong ferrite stabilizer, and acts as a solid solution strengthener. It diffuses slowly and slows down the recovery and precipitation process, produces more stable microstructure by slowing down the recovery of martensitic structure. Depending upon the other ferrite and austenite stabilizers present in the steel the amount of W must be limited to avoid δ-ferrite. Higher amount of W in steel causes formation of laves phase when the steel is exposed to temperatures around 600°C. This laves phase is fine and uniformly distributed and contributes to strengthening but its thermal stability is very poor so it dissolves in matrix eventually to give away stable precipitates. Its low radioactivity made it an important alloying element in the RAFM steels [58]

Vanadium (V) is a ferrite stabilizer. It is added to the steel to form MX type of carbides, nitrides and carbonitrides (where M = V, Ta and X = C, N) which contributes significant increase in creep strength. These carbides and/or nitrides are stable at temperatures more than 1000°C [6,17]**.**

Tantalum (Ta) has tendency to form carbides, almost equal to that of V. In W containing steels, Ta addition proved retardation of the growth of Laves phase. Its lower radioactivity has made it an important alloying addition in the RAFM steels.

Silicon (Si) is a ferrite stabilizer. If present in minor quantities, it increases the flowability of the steel when it is in the liquid form. It also acts as a deoxidizer of the steel. Like Cr, silicon improves oxidation resistance of the steel. However, it enhances the precipitation of Laves phase
Manganese (Mn) has the greatest effect on hardenability of the steel out of all the alloying elements. However, greater amounts of Mn have adverse impact on creep strength.

Nitrogen (N) is necessary for the formation of nitrides and carbo-nitrides. It also ensures the matrix fully austenite during homogenisation. When present in quantities greater than 0.015 wt. %, it tends to form nitrides with elements like, Ti, V, Cr, etc. In boron containing steels, the amount of N is further restricted as it promotes the formation of boron nitride inclusions at grain boundaries

2.6. Various type of precipitates in ferritic steels

Depending upon the composition, temperature and time of exposure different types of precipitates have been identified in ferritic steels. The volume fraction of these precipitates also varies due to straining action. Various types of precipitates in ferritic steels include $M_{23}C_6$, MX (where M = V, Ta and X = C or N), M_3C, M_2C, M_6C, Laves and Z phases. Among all these precipitates, $M_{23}C_6$ and MX precipitates are thermodynamically stable. Others precipitates (M_3C, M_2X and M_6C) are unstable and give away within a short duration of time. Laves and Z phases form during prolonged service exposure at a particular range of temperatures and are considered to be detrimental to creep strength.

a) **$M_{23}C_6$:** These precipitates are of face centered cubic and their formation is favored in high Cr steels. These carbides mainly consist of $Cr_{23}C_6$. However, solubility of other elements is also reporte. In RAFM steels, $M_{23}C_6$ contains Cr, W and Fe as major elements and a small amount of V is also reported [12]. Enrichment of Cr is reported in 9Cr classes of steels as it grows. These precipitates remain stable during long term service in the temperature range of 773 to 1033 K. Considerable coarsening of the carbide phase is reported to soften the ferrite matrix. Addition of W to RAFM steel is reported to control the coarsening of $M_{23}C_6$. Fine precipitates of $M_{23}C_6$ are beneficial in increasing the strength of the steel by pinning the grain and sub-grain boundaries. However, the coarsening of these carbides during creep exposure leads to the recovery of dislocations and coarsening of lath structure and results in a decrease in resistance to creep deformation.
b) **MX:** These precipitates are also face centered cubic and forms at intra-lath regions. These precipitates are carbides/carbonitrides of V and Ta. Unlike $M_{23}C_6$, these precipitates are highly stable up to 1681 K. These carbides/carbonitrides do not coarsen significantly during prolonged thermal exposure and even under creep exposure. Therefore, these carbides are accountable for the high temperature strength of the steel during prolonged service.
c) **M_2X:** The precipitate M_2X is a nitrogen rich phase and forms at the expense of Laves (Fe_2W) and Z phases [(Cr, Ta)(C,N)] at low temperature (< 873K). M_2X precipitate is stable at low temperature compared to the Cr rich $M_{23}C_6$. However, it is unstable during longer durations of thermal exposure. The possibility of formation of M_2X precipitate is favourable in steels with more than 0.1 wt% of nitrogen. In case of RAFM steel, the N content is restricted to 0.0226 wt% due to radiological safety considerations. Thermodynamic

calculations show that Cr_2N precipitate exists within a narrow temperature window with a volume fraction of ≈ 0.02% [46,54].

d) **M_3C:** M_3C carbides are iron-rich precipitates with complex orthorhombic structure. The formation of M_3C carbides are well known in low chromium steels. These carbides are not expected to form in 9Cr class of steels. However, the precipitation of iron-rich M_3C carbide has been reported in normalized steel. Thermodynamic calculations shows that the M_3C precipitate is not a stable phase in 9Cr steels

e) **Z-phase:** Z-phase is a complex tetragonal nitride with the general formula Cr(X)N, where X= Ta, V. Z phase forms with the dissolution of the cubic MX precipitates. It coarsens much faster than the MX precipitate. While the increase in resistance to creep deformation is attributed to the existence of MX precipitates in the matrix [67], the formation of Z phase lead to a steep reduction in the creep rupture strength of the higher chromium ferritic steels.

f) **Laves Phase:** Other than carbides or nitrides, the precipitation of laves phase is reported in 9Cr creep resistant steels containing Mo or W during low temperature thermal exposure, viz. aging and creep. At 600°C and above, laves phase quickly coarsen and this coarsening is much faster when the steel is subjected to higher stresses. Formation of lave phase removes the solid-solution strengthening elements such as W and Mo from solution. While the formation of fine precipitates of laves phase is beneficial and increases the strength of the steel, its rapid coarsening during thermal exposure is detrimental to the mechanical properties of the steel, especially toughness. In RAFM steels, the formation of laves phase depends on the W content of the steel. Increase in W content increases the formation of laves phase

g) **Chi (χ)–phase:** The Chi (χ) phase is a metallic phase that occurs at lower temperatures especially in non corroding steels consisting of high chromium concentrations. The χ phase is undesirable as which promotes embrittlement, reduces the ductility and corrosion resistance of the steel. The Chi (χ) phase metallographically designated as $M_{13}C$/ $Fe_{13}Cr_{12}M_{10}C$ and consists of BCC structure. By selection of proper heat treatments can avoid the diffusion of Chi phase.

2.10. Thermomechanical treatment and related literature:

The principle behind the TMT processing is that the plastic deformation of metastable austenite leads to creation of defects in the steel. The defects might be in the form of dislocation and stacking faults. These defects are retained during quenching which is subsequent to TMT and these faults acts as nucleating sites for formation of precipitates. The basic objective of the TMT is to improve the mechanical properties of the material without losing or even sometimes improvement in the ductility. This is the basic requirement of the steel for fabrication of test blanket modules for ITER. There are many efforts in progress to increase the microstructural stability of the steel by TMT as an alternative to change in chemical composition**.** Earlier investigations on modified 9Cr-1Mo steel showed enhanced precipitation of nano-sized MX type precipitates over $M_{23}C_6$ on TMT processing, thus increasing the resistance to creep deformation and rupture life**.** However, very limited studies have been carried out on RAFM steel using TMT for improving the creep rupture life. Significant variables that influence the final microstructure of TMT steel greatly are: temperature of deformation, percentage of deformation, strain/ strain rate, type of deformation (cold/warm/hot working) and time and temperature of subsequent ageing. A good number of attempts have been made by using TMT on quite a few ferritic, ferritic/martensitic steels and these are appended below with the gaps identified.

Thermomechanical treatment of P91 steel by warm rolling in metastable austenitic phase was studied by **S. Hollner et al.** [25]. The warm rolling of P91 steel was carried out at 600°C with 25% reduction in thickness followed by tempering at two temperatures, 650°C and 700°C **(Fig.2.6)**. It is reported that TMT of the steel led to the refinement of martensitic structure and the dislocations are pinned by large number of carbide and nitride precipitates **(Fig.2.5)**. As a result, great improvement in yield strength and ductility were observed after TMT (**Fig.2.7).** Substantial improvement in creep life of P91 steel was also reported. However, these researchers have not studied the effect of ageing on tensile and creep properties of the steel after TMT.

In an another study carried out by **Shengzhi Li et al.** on commercial P92 steel, the TMT was done at 650°C with 75% and 93% reductions in thickness followed by tempering at 650°C, 700°C and 765°C for 60 min. Post microstructural investigations indicate that there is vast improvement in nano sized precipitates (i.e. $M_{23}C_6$ and MX) **(Fig.2.8)** compared to those in as-received P92 steel. Thus, resulting in significant improvement in tensile and creep rupture strength properties **(Fig.2.10** and **2.11)**.

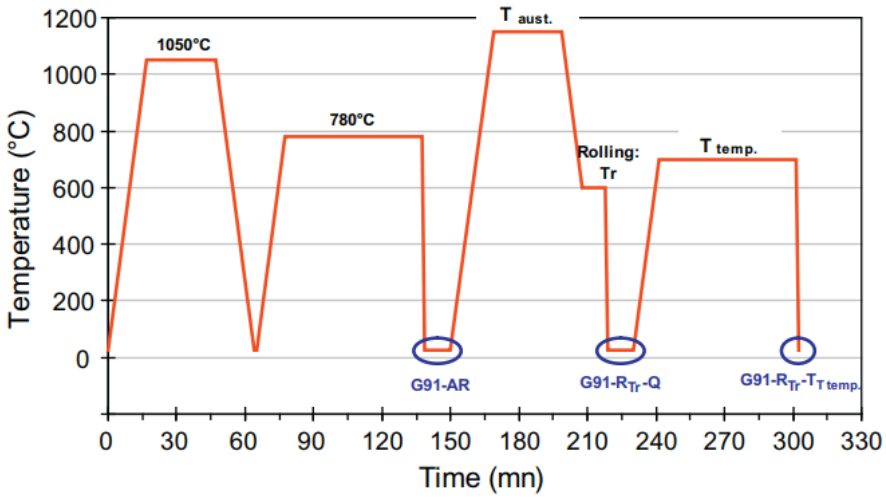

Fig.2.6. TMT of P91 grade steel (AR- as received, R-rolled, Q- quenched and T- tempered). **S. Hollner et al.** [25]

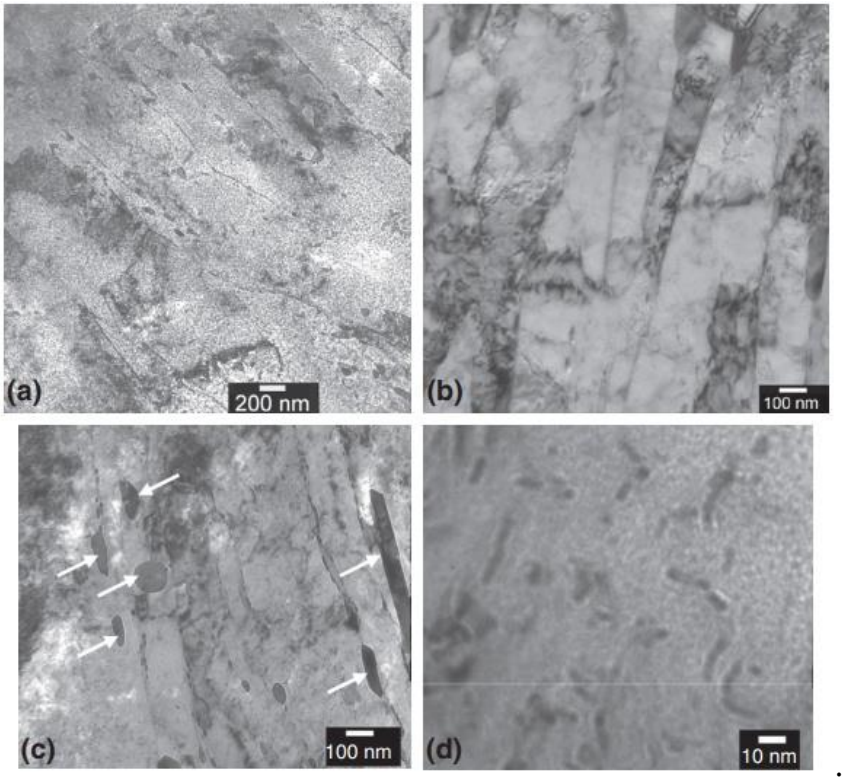

Fig.2.7. TEM images of P91 steel subjected to warm-rolling at 600°C at different tempering temperatures. (a) tempering at 650°C, (b) tempering at 700°C. Showing fine lath structure with distribution of $M_{23}C_6$ and MX precipitates. (c) $M_{23}C_6$ precipitates (d) MX precipitates inside the lath matrix. **S. Hollner et al.** [25]

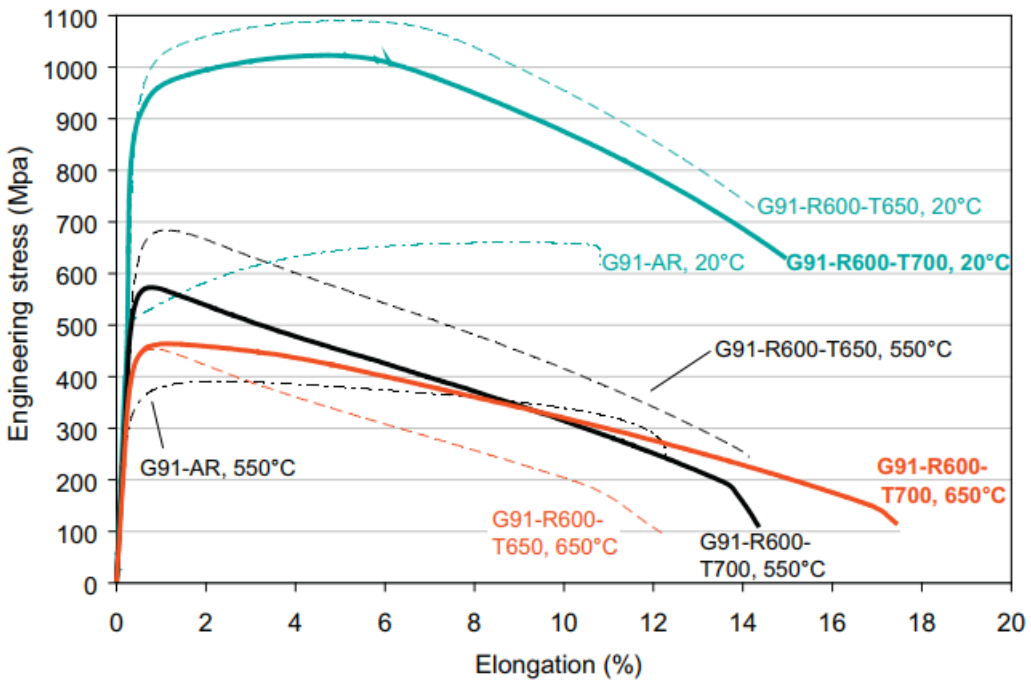

Fig.2.8. Tensile properties of P91 grade steels subjected to TMT. **S. Hollner et al.** [25]

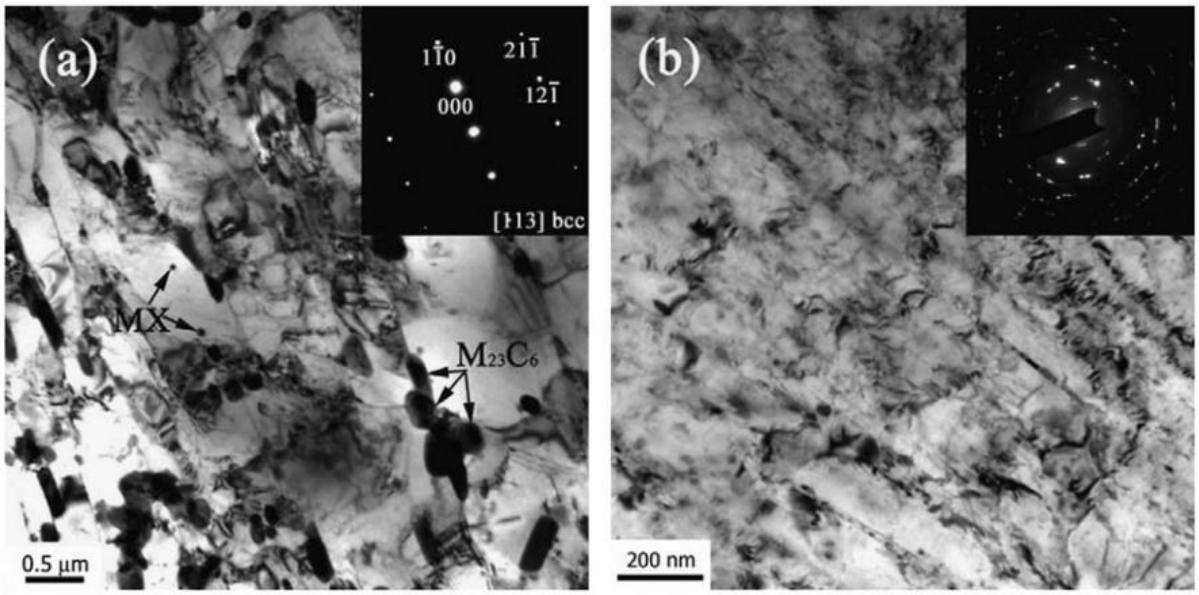

Fig.2.9. TEM images of P92 steel in **(a)** as received condition **(b)** TMT at 600°C with 93% reduction in thickness.

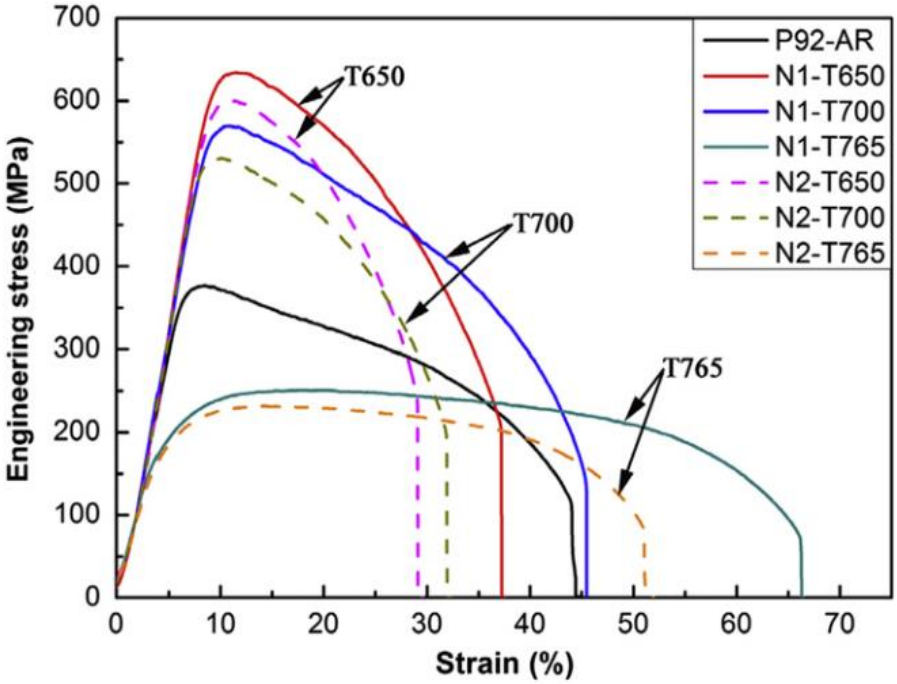

Fig.2.10 Engineering stress-strain curves of P92 steel in as received and TMT conditions tensile tested at 600°C. **Shengzhi Li et al.** [10]

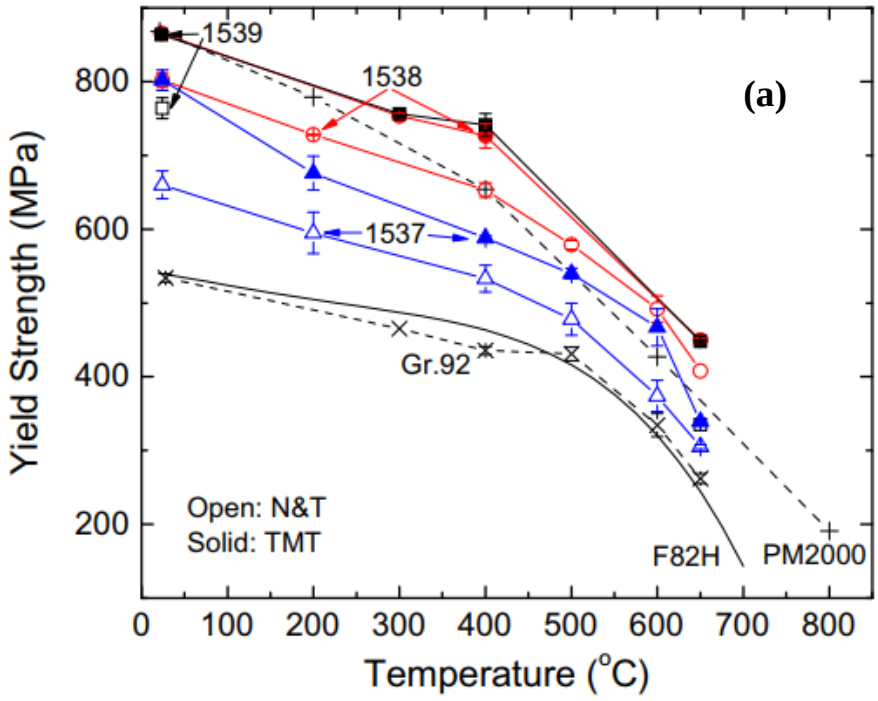

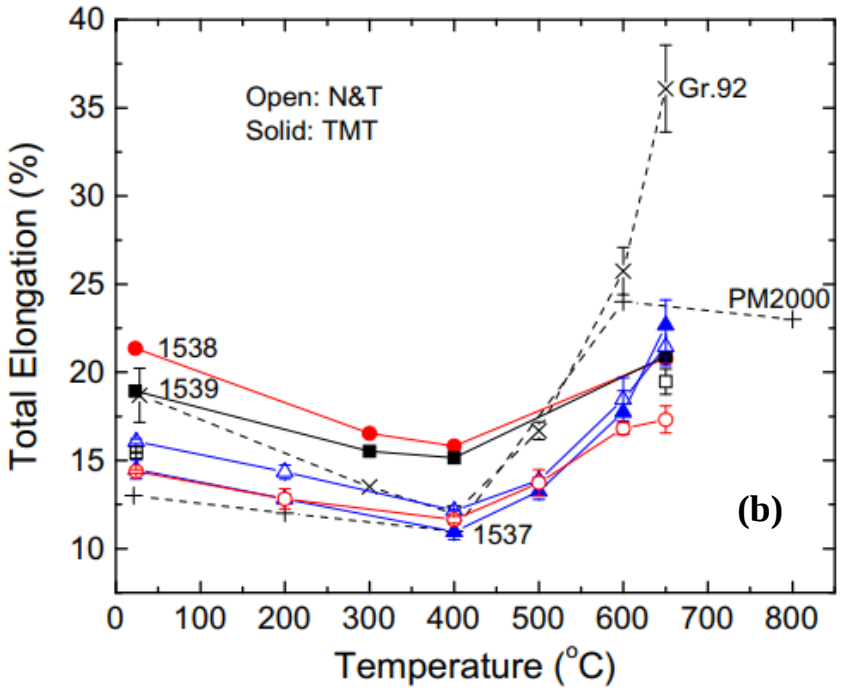

Fig.2.11. Comparison of **(a)** yiled strenth and **(b)** elongation properties of different heats of RAFM steel (1537, 1538 and 1539) in N+T and TMT conditions with the literature data of other grades ferritic steels i.e. P92, ODS steel PM2000 and F82H. **L.Tan et al.** [24]**.**

CHAPTER 3

EXPERIMENTAL PROCEDURES

3.1. Thermomechanical treatment (TMT)

The RAFM steel in normalized and tempered condition (N+T) is taken as the starting material for the thermomechanical treatment (TMT). TMT is the process which involves simultaneous application of heat and deformation to the material in order to change morphology of the precipitates and modify the microstructure. In the present study, TMT has been performed to the steel in two different phase field conditions, viz. (i) austenitic phase field and (ii) ferritic phase field conditions to understand the microstructural, mechanical and creep rupture behaviour of the steel. The suitable temperature and time for carrying out the TMT were identified from the phase diagram and CCT diagram developed by using Thermo-Calc and dilatometry studies respectively (discussed in results chapter). From these studies, the deformation (warm-rolling) temperature was fixed as 700°C and at this temperature the soaking time determines the phase field. For TMT in austenitic phase field, the steel was first warm-rolled at 700°C and rolling time was maintained well within 10 min; whereas for TMT in ferritic phase field, the steel was first soaked for 120 min at 700°C to bring it into ferritic phase and then warm-rolled.

Figures 3.1 illustrates the sequence of heat treatment and processing steps used for TMT in austenitic and ferritic phase field conditions and subsequent tempering. Prior to TMT, the steel was subjected to austenitization at 1423 K for 10 min to convert tempered martensite to austenite and dissolve the existing precipitates and then cooled in air (≈ –1 K/s) to the warm-rolling temperature (973 K). In austenitic phase field condition, the warm rolling was carried out immediate to the austenitization followed by cooling to 973 K; where as in ferritic phase field condition after the initial austenitization the steel was cooled to 973 K and maintained there for 120 min to fully convert the steel from austenite phase to ferritic phase condition. The timings were decided based on the dilatometry experimentation and from the literature. The warm-rolling was carried out using a 200 ton capacity, two-high rolling mill (Make: DEMAG) **(Fig.3.2)** with a roll diameter of 300 mm. The warm-rolling process was completed within 10 minutes. During warm-rolling, a reduction of 25% in thickness was imparted in five passes. The plate was reheated to its original warm-rolling temperature (973 K) after each pass as the temperature of

the plate was dropped. After completion of warm-rolling, two additional passes were given to the plates without any reduction for straightening. Subsequent to warm-rolling, the plates were aged at rolling temperature (973 K) for 30 min to provide sufficient time to nucleate, grow and stabilization of precipitates in austenitic phase field condition. Prolonged soaking at aging temperature may lead to the formation of ferrite due to transformation kinetics, i.e. ferrite does not form in 40 min. Hence, the aging time was limited to 30 minutes. However, in ferritic phase field condition the ageing was not carried out on the steel after warm-rolling process and the steel was air cooled to room temperature. Subsequently, the steel was subjected to tempering at 1038 K for 90 min for both the phase field conditions.

Coding of the samples:

N+T : Normalized and Tempered condition

AF-TMT25 : TMT in austenitic field condition followed by ageing and tempering

FF-TMT25 : TMT in ferritic field condition followed by tempering

The number 25 refers to 25% deformation during TMT.

Note: TMT25 refers both AF-TMT25 & FF-TMT25

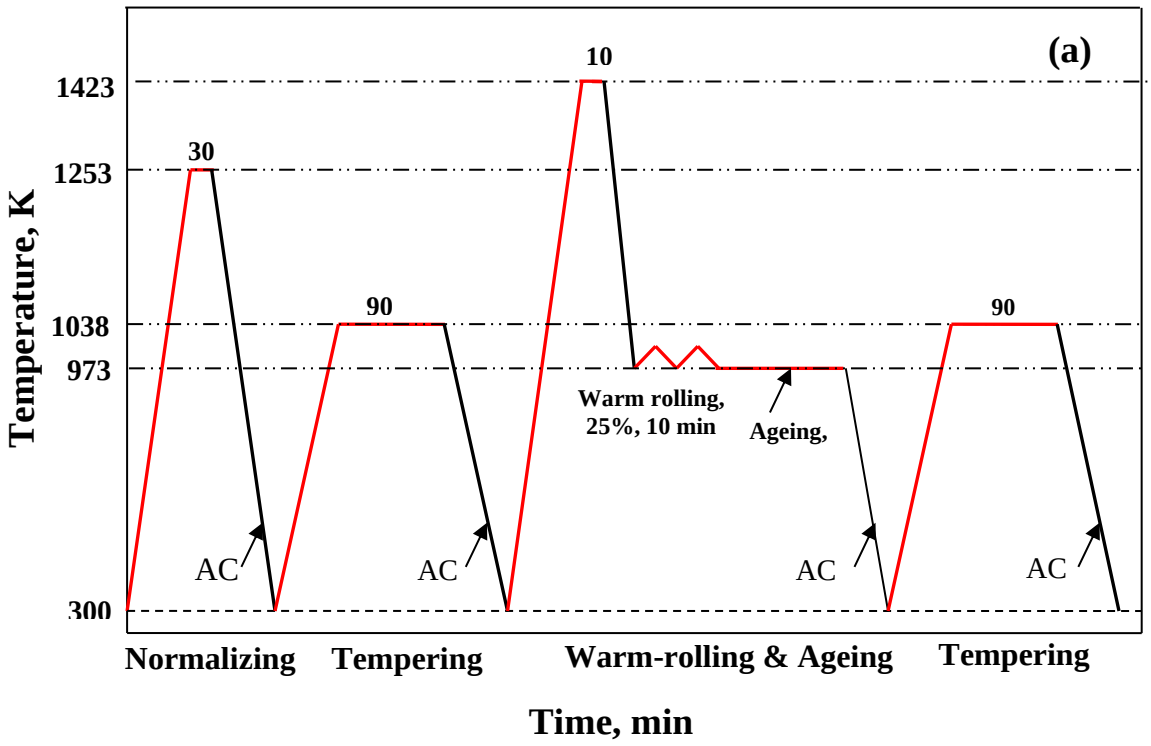

Fig.3.1. Normalizing and tempering followed by thermomechanical treatment cycle used for RAFM steel in austenitic phase field (X and Y- axes are not to scale)

Fig.3.2. DEMAG hot rolling mill at DMRL, Hyderabad

3.6. Microstructural investigation

Microstructural studies of RAFM steel were carried out by using optical and electron microscopy. Microstructures were recorded in N+T and TMT conditions of steel in prior to test condition and post-tensile and post-creep test conditions.

3.6.1. Optical microscopy (OM):

Optical microstructures of RAFM steel in N+T and TMT25 conditions were obtained by using Leica metallurgical microscope (Make: Leica, Model: DMi8A) equipped with image analysis software (Leica Application Suite (LAS). Representative samples of dimensions 10 × 10 × 10 mm were cut from RAFM steel in N+T and TMT25 conditions for metallography by using linear precision saw (Make: Buehler, Model: Isomet 4000). The samples were polished successively on 400, 800, 1200, and 2000 grit silicon carbide emery papers. This was followed by polishing to mirror finish using diamond paste up to the size of 1 µm on velvet cloth. The mirror finished samples were etched for 10-15 s using Villela's reagent (1 g picric acid and 5 ml hydrochloric acid in 100 ml ethanol). Magnification images along with EDS analysis of the matrix and the precipitates, wherever required, were obtained. These high magnification images of both SEM and FEG-SEM were well utilized in quantifying the precipitates (before and after testing) in both conditions of the steel. The fractography of the tensile and creep failed samples was also carried out by using SEM.

3.8.3. Tensile tests:

Tensile tests were carried out on RAFM steel in N+T and TMT25 conditions using Hung-Ta tensile testing machine (model: HT-2402, capacity: 10 ton) in the temperature range of 300 - 923 K and at a nominal strain rate of 3×10^{-4} s^{-1}. The tensile testing machine is equipped with a 3-zone resistance heating furnace and digital data acquisition system. Cylindrical threaded type tensile specimens of 5 mm gauge diameter and 25 mm gauge length were used, according to ASTM E8M standard to carry out the tensile tests. Separate temperature controllers were used to maintain constant temperature across the different zones of the furnace. K-type thermocouples were used to monitor the temperature of the test specimen. Prior to tensile testing, the specimen was heated to test temperature. The specimen was held for 15 min at test temperature to ensure uniform temperature along the specimen within ±2 K. Load-elongation data were recorded using

digital data logger. The geometry of the specimen before and after tensile tests is shown in Fig. 3.3

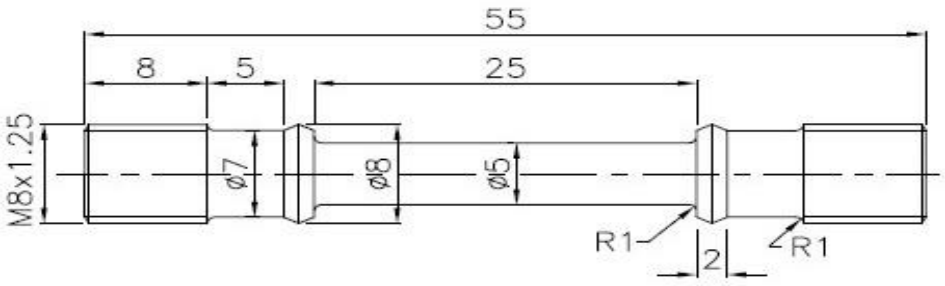

Fig.3.3. Schematic of standard tensile test specimen (as per ASTM E8M)

Chapter-4
Experimental Results

Microstructure:

4.1. Optical and electron back scattered diffraction (EBSD) microstructures of RAFM steel in N+T, AF-TMT25 conditions:

The optical microstructures of RAFM steel in N+T, AF-TMT25 conditions are shown in **Figs.4.1a** mages are presented adjacent to them in **Figs.4.1b** respectively. While the steel in N+T condition reveal completely tempered martensitic structure within prior austenite grains (PAGs), the steel in AF-TMT25 condition shows tempered martensitic structure with traces of ferrite along the PAGs. The coarsening of PAG in TMT25 steel could be due to renormalizing the steel to higher temperature where the prior existing precipitates dissolved paving the way for grain coarsening. The small amount of ferrite phase seen along the PAGBs of the AF-TMT25 steel was also confirmed by the micro-hardness (180-190 HV) measurements. Nucleation of ferrite phase along the PAGBs can be justified as the imposed deformation and hold time (i.e. ageing time) might have led the steel incursion into the $\alpha+\gamma$ phase field during ageing. Similar observation of ferrite phase formation along the PAGs during TMT has been reported by **Matthias et al.**[13]. The imparted deformation (reduction in thickness) is expected to induce more nucleation of ferrite due to high driving force for austenite to ferrite transformation Longer isothermal ageing time at 973 K is also expected to transform more austenite into ferrite. In the present case, an isothermal holding time of 30 min was chosen after TMT. Probably, this hold time could be slightly more for the steel subjected to 25 % reduction in thickness (TMT25) thereby promoting the formation of ferrite along PAGBs. Expected fine dispersion of large number of precipitates along the grain boundaries and within the austenite matrix **(**discussed in section 4.4.2) might have also acted as nucleation sites for ferrite formation during ageing. Formation of ferrite along the PAGB on high temperature normalization in RAFM steel has also been reported by **Chandravathi et al.**

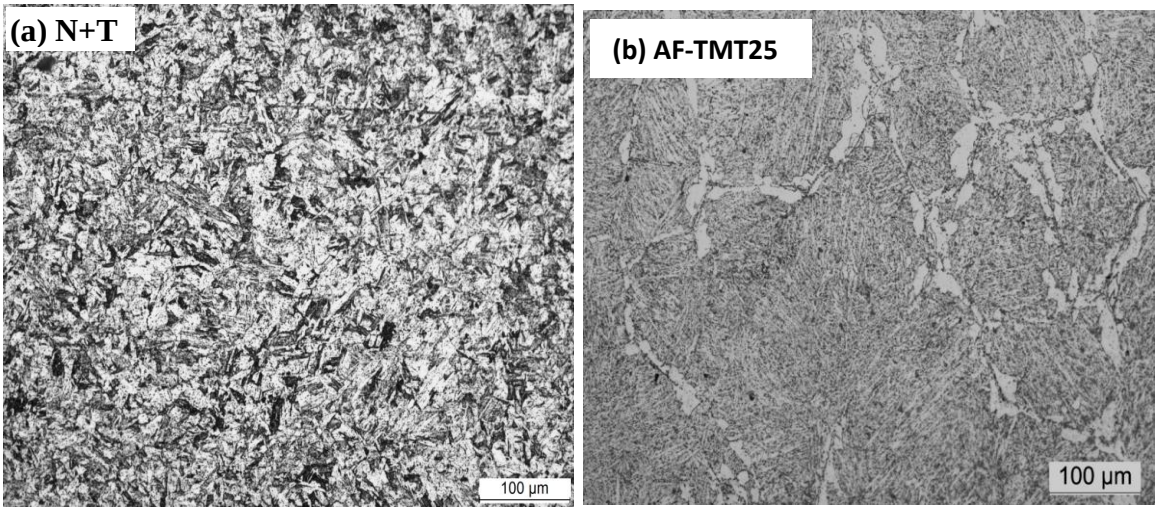

Fig.4.1. Optical and EBSD microstructures of RAFM steel in **(a)** N+T **(b)** AF-TMT25

4.5.2. Scanning Electron Microscope (SEM)

Figures 4.2a shows the FESEM images of RAFM steel in N+T, AF-TMT25 conditions. The typical tempered martensitic structure decorated with $M_{23}C_6$ precipitates along the PAG and MX precipitates within the matrix of the RAFM steel in N+T and AF-TMT25 conditions. However, the steel in FF-TMT25 condition exhibited fully ferritic structure with numerous $M_{23}C_6$ precipitates along the PAG and finer MX precipitates within the matrix. In N+T condition (**Fig.4.2a**) the whole PAGs are clearly visible as its size is smaller, whereas in TMT25 condition (**Fig.4.2b**) the image covers a small portion of the PAG for the same magnification but showing the increased quantity of refined precipitates than in the N+T condition. The increase in prior austenite grain (PAG) size relies on the selection of re-austenitization temperature and the rate of deformation in TMT. The similar features were reported by Matthias et al. [16] and Sakthivel et al. [35].

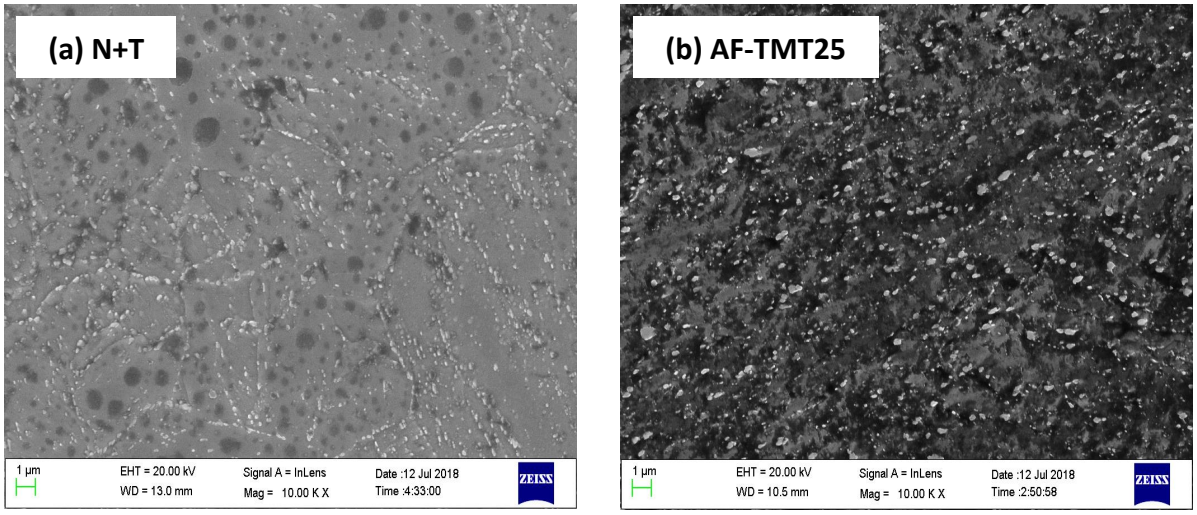

Fig.4.2. FESEM images of RAFM steel in **(a)** N+T **(b)** AF-TMT25

CHAPTER 5

HARDNESS AND TENSILE BEHAVIOUR

This chapter describes the hardness and tensile properties of RAFM steel subjected to thermomechanical treatment (TMT) in two phase field conditions, namely (i) austenitic phase field condition (AF-TMT25) and (ii) ferritic phase field condition (FF-TMT25). The competent results obtained on RAFM steel in both TMT conditions were compared with those results obtained on traditional normalized and tempered (N+T) condition. The tensile tests were performed on the steel in all three conditions, viz. N+T, AF-TMT25 and FF-TMT25, in the temperature range of 300-923 K and at a strain rate of 3×10^{-4} s^{-1}. The tensile flow behaviour of RAFM steel has been assessed using various constitutive equations, namely (i) Hollomon , (ii) Ludwik (iii) Ludwigson and (iv) Voce equations**.** The strength related parameters of the Voce constitutive equation, namely initial stress and saturation stress are compared for all three conditions of the steel. The variations in strength, ductility, reduction in area of RAFM steel in three conditions are correlated with corresponding microstructural features of the steel. In this chapter, the tensile test results obtained on RAFM steel subjected to TMT in two phase field conditions, i.e. AF-TMT25 and FF-TMT25 are discussed separately while comparing with N+T condition simultaneously.

HARDNESS

Systematic investigation of hardness of the RAFM steel at different stages of TMT was carried out to obtain more insight of the steel. The hardness of the steel in N+T, TMT with and without tempering and ageing in austenitic & ferritic phase field conditions is obtained and the results are compared and discussed.

5.1. Hardness of RAFM steel in N+T condition

The hardness of the RAFM steel in normalized condition (1253 K for 30 min) is found to be 375±2 HV_{10}. This high hardness can be attributed to the presence of fully martensitic structure with high dislocation density. Upon tempering, the hardness of the steel is reduced to 206±2 HV_{10} due to recovery of the dislocation structure.

5.2. Effect of TMT in austenitic phase field on hardness

The hardness of the RAFM steel after normalizing and tempering is found to be 206±2 HV_{10}. Upon TMT (warm rolling) followed by ageing at warm rolling temperature, the hardness is

increased to 365±2 HV_{10}. Later, on subjecting to tempering, the hardness is reduced to 222±2 HV_{10}. The comparison of the Vicker's hardness values of the RAFM steel in N+T condition, AF-TMT25 without and with tempering conditions are shown in **Fig.5.1**. The imparted deformation in austenitic phase field, enhanced precipitation of $M_{23}C_6$ and MX during ageing upon deformation and formation of martensite structure on cooling are expected to increase hardness of the TMT processed steel over that in N+T condition. However, formation of small amount of ferrite phase during TMT is expected to reduce the hardness. Hardness of the steel in usual normalized condition (1253 K for 30 min) was around 375±2 HV_{10}. Considering this, the TMT has decreased hardness of the steel. During TMT, locking of carbon as precipitates decreased the hardenability of the steel drastically resulting in decrease in hardness of the martensite steel, which could not have been recovered by the expected enhanced precipitation and imparted deformation. The decrease in hardness is associated with reduction in martensitic transformation induced dislocations [82]**.**

5.3. Effect of TMT in ferritic phase field on hardness

The Vicker's hardness values of the steel in ferritic phase condition, without and with tempering, are compared with the N+T condition and is shown in **Fig.5.1**. The macro Vickers hardness values are raised to 409±2 HV_{10} upon TMT without tempering from 206 HV_{10} in N+T condition.

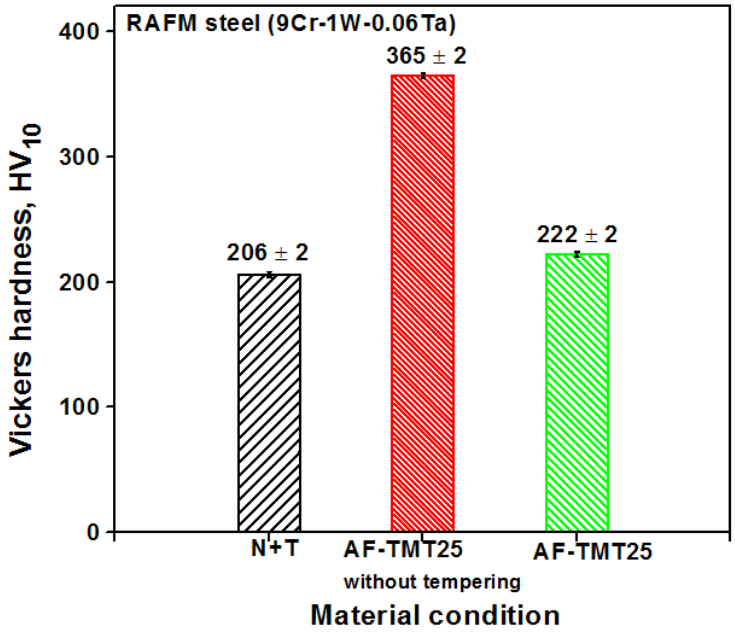

Fig.5.1. Comparison of the Vicker's hardness values of the RAFM steel in N+T condition, AF-TMT25 without and with tempering conditions.

TENSILE BEHAVIOUR

AUSTENITIC PHASE FIELD CONDITION

5.4. Effect of TMT on tensile flow behaviour

The engineering stress-strain curves of RAFM steel in N+T and AF-TMT25 conditions tested in the temperature range of 300 - 923 K at a strain rate of 3×10^{-4} s^{-1} are shown in **Figs.5.2** and **5.3** respectively. The steel in both conditions exhibited monotonic stress-strain curves over the entire temperature range with no indication of serrated flow in the intermediate temperature range as commonly observed in such ferritic steels. While the strength of the RAFM steel, in both N+T and AF-TMT25 conditions, decrease gradually with progressive increase in temperature; the strain to failure (e_f) decrease up to 673 K and beyond which it increased in both conditions.

5.5. Effect of TMT on yield and ultimate tensile strengths:

The variations of 0.2% offset yield strength (YS) and ultimate tensile strength (UTS) with temperature of the RAFM steel in both N+T and AF-TMT25 conditions are shown in Figs **5.4.** respectively**.** TMT of the steel increased both YS and UTS over the temperature range investigated. The variations of YS and UTS with temperature exhibit sudden decrease in stress from 300 K to 473 K followed by gradual decline in intermediate regime (473-723 K) and followed by rapid decrease at high temperatures. In the present investigation of TMT of RAFM steel, both the high and low temperature tensile strengths are appreciably increased. Microstructural refinement of the steel in terms of lath size and more amounts of fine precipitates apart from high retained dislocation are considered for the improvement in tensile strength of the steel on TMT.

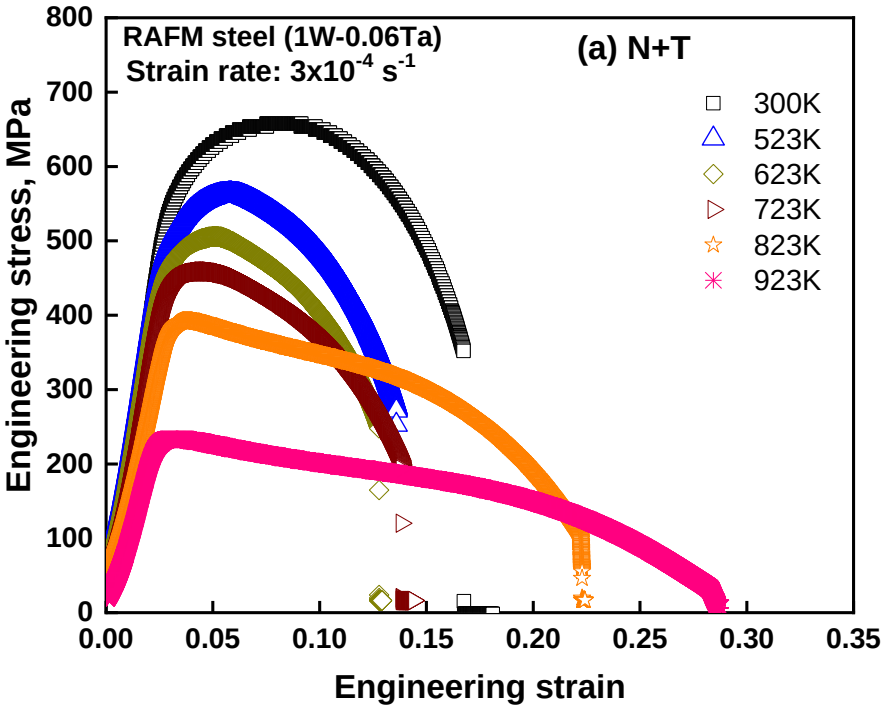

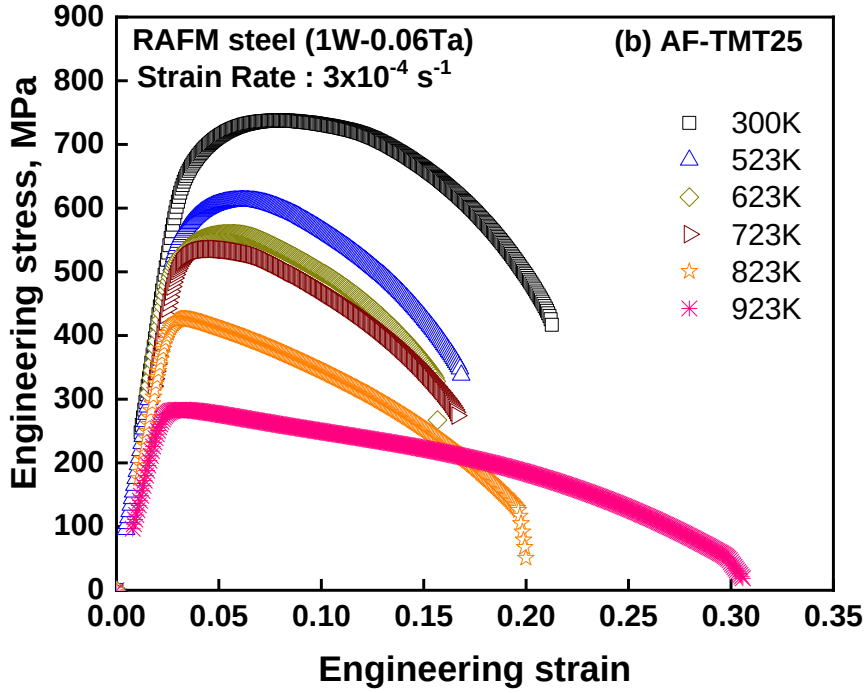

Fig.5.4. Tensile curves of RAFM steel at different test temperatures at strain rate of 3×10^{-4} s^{-1} for **(a)** N+T and **(b)** AF-TMT25 conditions.

5.6. Analytical framework:

5.6.1. Constitutive flow behaviour:

In order to understand and justify the performance of the reactor structural components, it is essential to have a broad understanding in the area of high temperature tensile flow behaviour of the engineering structural materials. Several renowned investigators like Hollomon, Ludwik, Ludwigson and Voce have proposed constitutive relationships for describing the plastic flow behaviour of engineering materials in different material conditions. Extensive studies have been carried out by many researchers to understand the tensile flow characteristics of engineering materials using constitutive equations and to describe the physical significance of the parameters used in the equations. The following are the most significantly used constitutive flow equations:

a) Constitutive equation proposed by Hollomon It is a simple power law relation between true stress (σ)-true plastic strain (ε) and is expressed by

$$\sigma = K_H \varepsilon^{n_H} \tag{5.1}$$

where K_H is the strength coefficient and n_H is the strain hardening exponent. This relation provides a measure of uniform elongation and ultimate tensile strength through n_H and K_H, respectively.

***b) Constitutive equation proposed by Ludwik*:** It is expressed by

$$\sigma = \sigma_o + K_L \varepsilon^{n_L} \tag{5.2}$$

Where σ_0 is a material constant which accounts for the positive stress deviation owing to yielding at low strains, K_L is the strength coefficient and n_L is the strain hardening exponent.

***c) Constitutive equation proposed by Ludwigson*:** Ludwigson demonstrated that flow behaviour of many face centered cubic (FCC) metals and alloys having low stacking fault energy cannot be described by simple Hollomon equation (Equation 5.1) due to large positive stress deviation at low strains. He suggested that the positive stress deviation at low strains can be overcome by an additional term, and is expressed as

$$\sigma = K_1 \varepsilon^{n_1} + \exp(K_2 + n_2 \varepsilon) \tag{5.3}$$

where K_1 and n_1 are the strength coefficient and strain hardening exponent respectively, and K_2 and n_2 are additional constants.

***d) Constitutive equation proposed by Voce*:** For materials exhibiting saturation in stress at high stress/strain levels, Voce proposed a flow relationship as

$$\sigma = \sigma_S - (\sigma_S - \sigma_I)\exp\left(\frac{-(\varepsilon - \varepsilon_I)}{\varepsilon_c}\right) \quad (5.4)$$

where σ_S is the saturation stress, σ_I and ε_I are true stress and true plastic strain at the onset of plastic deformation (i.e. initial stress and initial strain) respectively, and ε_c is a characteristic strain constant. For condition $\varepsilon_I = 0$, equation 5.4 reduces to

$$\sigma = \sigma_S - (\sigma_S - \sigma_I)\exp(n_V \varepsilon) \quad (5.5)$$

where $n_v = -1/\varepsilon_c$

The constant n_V determines the rate at which the stress tends to reach steady state value, and σ_s is expected to be close to the value of UTS. In this approach, the flow curve is viewed as a transient of the flow stress from some initial value to the saturation value.

5.7. Effect of TMT on constitutive flow behaviour:

In the present investigation, a comprehensive attempt has been made to describe the tensile flow and work hardening behaviour of RAFM steel subjected to thermomechanical treatment for wide range of temperatures (300-923 K) at a strain rate of 3×10^{-4} s^{-1} under the framework of most commonly used constitutive equations. The data obtained by tests conducted on RAFM steel in TMT condition was compared with that obtained on the steel in normalized and tempered condition. Apart from all applicable flow equations, it has been demonstrated that the Voce equation provides adequate description of tensile flow behaviour of RAFM steel in both normalized and tempered and thermomechanical treated conditions in the range of temperatures of interest and strain rate for useful engineering applications.

Typical experimental log-log plots of true stress (σ) - true plastic strain (ε) for N+T and AF-TMT25 conditions along with the fitted flow curves as per the *Hollomon*, *Ludwik*, *Ludwigson* and *Voce* equations at 300 K (for low temperature), 673 K (for intermediate temperature) and only Voce equation at 873 K (for high temperature) are shown in **Figs.5.5** respectively. The values of χ^2 and minimum error band in determining the parameters of the different constitutive equations for RAFM steel in N+T and AF-TMT25 conditions are compared in **Table 5.1** and **Table 5.2** respectively**.** It can be observed that logσ-logε plots at low (300 K, **Fig.5.5**) and intermediate (673 K, **Fig.5.5** temperatures exhibit positive stress deviations at low strains from the extrapolated linear region at high strains for RAFM steel in N+T condition. The extent of positive stress deviation is observed to be decreasing with increasing temperature. But in case of AF-TMT25 condition, the experimental data showed almost

linear stress at all strains at low temperature (300 K, **Fig.5.5a**); whereas at intermediate temperature (673 K, **Fig.5.5b**) it showed linear stress at low strains and slightly negative deviation at higher strains. At higher temperatures (873 K, **Fig.5.5c**), stress-strain data on log-log scale of RAFM steel in N+T and AF-TMT25 conditions represents almost similar behaviour, indicating straight line at lower strains and curvilinear at higher strains with more deviation in AF-TMT25 condition compared to N+T condition. Hollomon and Ludwik parameters exhibits higher χ^2 values with higher error bands over all the temperature range. Even though Ludwigson equation exhibited smaller χ^2 values at par with Voce's relation, its error band is much higher than the Voce's band. It suggests that Voce's equation obeys adequately the stress-strain behaviour than the other constitutive equations used for the N+T and AF-TMT25 steels. The observed R^2 values **(Table 5.2)** are very close to unity in the case of Voce's and Ludwigson than the other two cases.

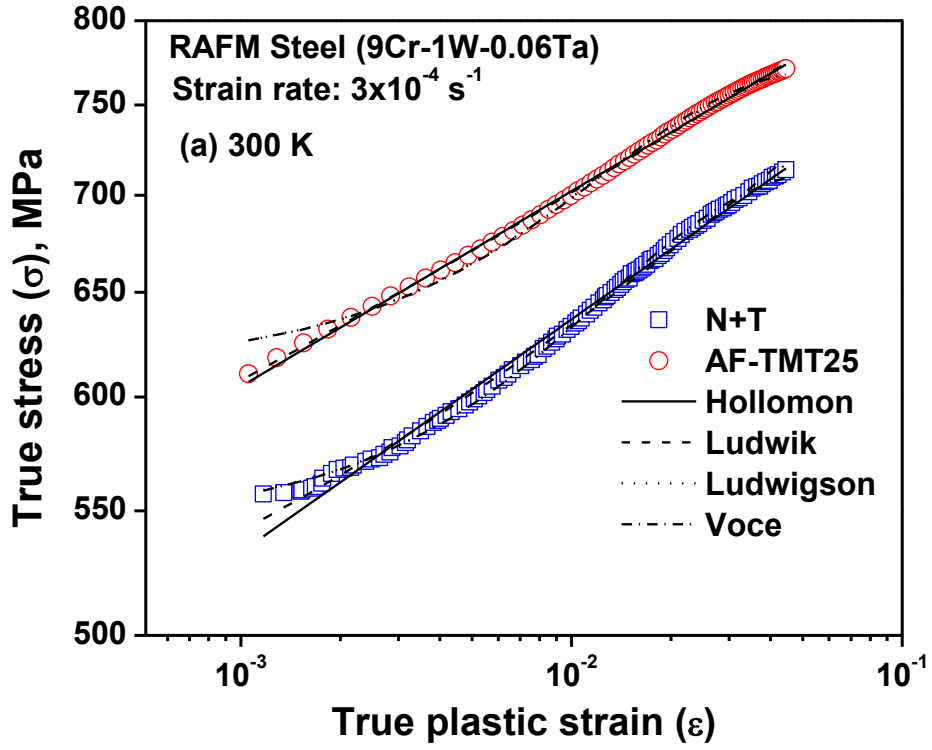
RAFM Steel (9Cr-1W-0.06Ta)
Strain rate: 3x10-4 s-1
(a) 300 K
N+T
AF-TMT25
Hollomon
Ludwik
Ludwigson
Voce
True stress (σ), MPa
True plastic strain (ε)
800
750
700
650
600
550
500
10-3
10-2
10-1

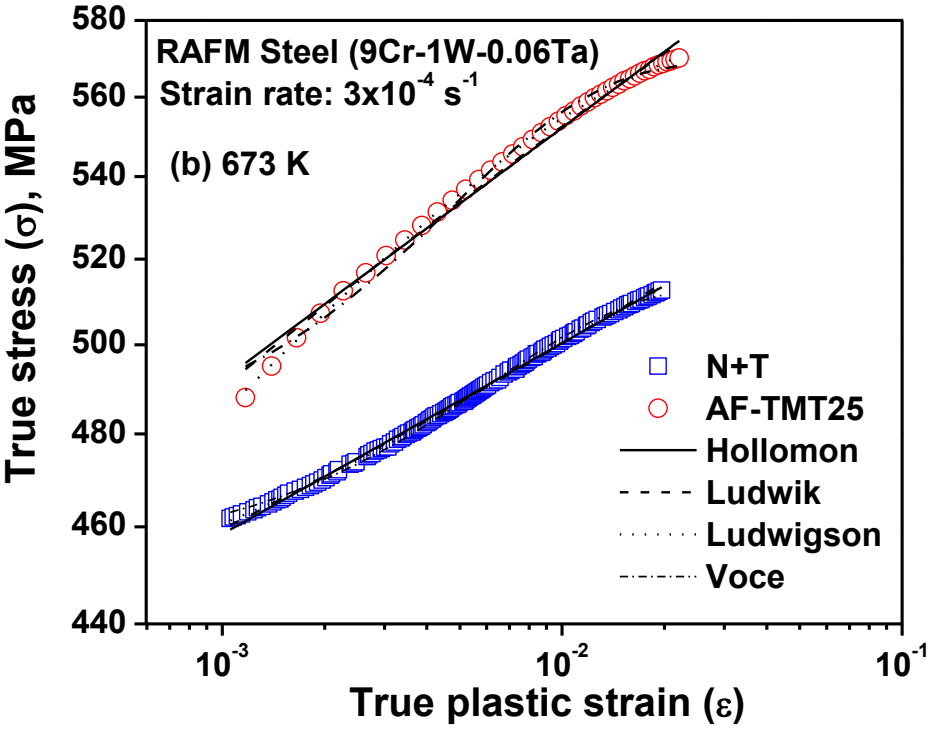
RAFM Steel (9Cr-1W-0.06Ta)
Strain rate: 3x10-4 s-1
(b) 673 K
N+T
AF-TMT25
Hollomon
Ludwik
Ludwigson
Voce
True stress (σ), MPa
True plastic strain (ε)
580
560
540
520
500
480
460
440
10-3
10-2
10-1

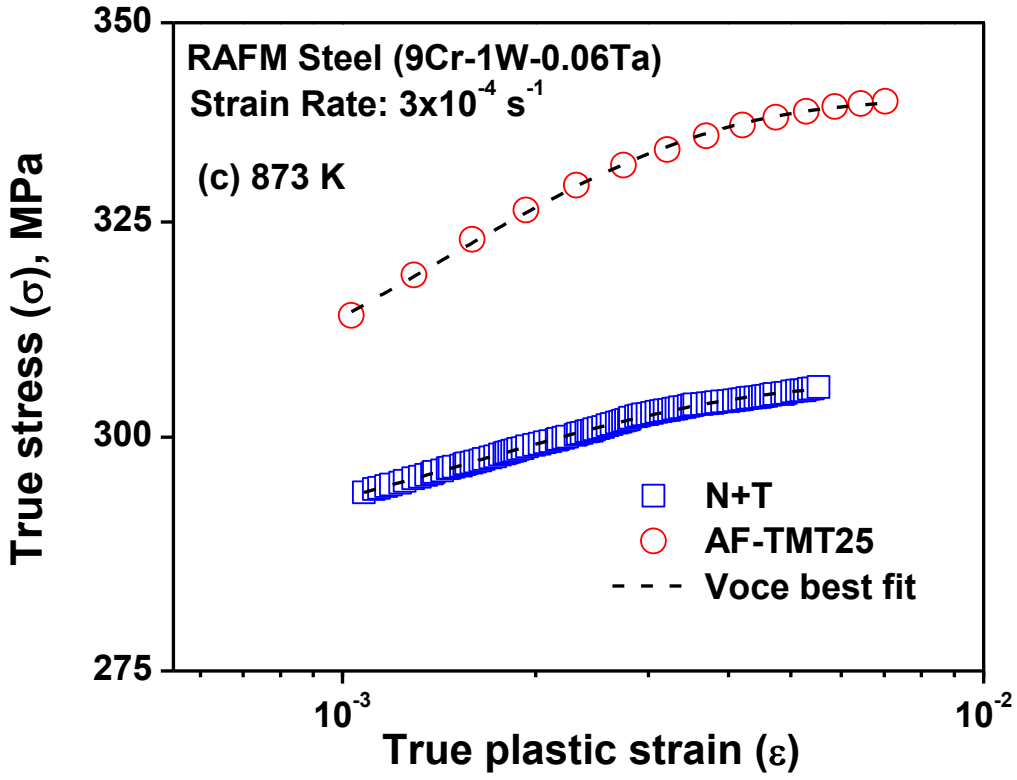

Fig.5.5. True stress-true plastic strain data of RAFM steel described by different flow equations at **(a)** 300 K, **(b)** 673 K, and **(c)** 873 K (Voce best fit) for both N+T and AF-TMT25 conditions .

Table 5.1

Typical χ^2 values obtained for different flow relationships in N+T and AF-TMT25 conditions of RAFM steel at all test temperatures

Temp, K	χ^2 values							
	Hollomon		Ludwik		Ludwigson		Voce	
	N+T	AF-TMT25	N+T	AF-TMT25	N+T	AF-TMT25	N+T	AF-TMT25
300	10.838	2.1258	10.281	2.0515	4.5585	0.4465	2.8697	1.531
473	2.647	1.9215	2.387	0.9879	0.4956	0.0496	1.1670	1.354
523	1.7963	1.1913	1.4340	0.8505	0.4391	0.0562	0.6844	0.1454
573	1.3737	0.8943	1.4831	0.6496	0.3214	0.0280	0.7031	0.2285
623	0.5666	0.9371	0.5990	0.7121	0.1682	0.0400	0.6238	0.1979
673	0.6129	1.9020	0.8677	1.6358	0.2557	0.0064	0.2607	0.1189
723	0.9036	1.9916	0.5410	1.8342	0.1264	0.0130	0.5204	0.0890
773	0.5405	2.3242	0.3326	2.3325	0.1273	0.0182	0.1810	0.0357
823	0.3329	1.8526	0.1745	1.9863	0.1414	0.2690	0.0748	0.0038
873	0.3831	0.2016	0.4063	0.2307	0.1200	0.0002	0.1104	0.0004
923	0.4079	1.4194	0.4049	1.4567	0.1547	0.0146	0.8163	0.0195

5.8. Voce's constitutive equation parameters:

The variations of the Voce's constitutive equation parameters σ_I, σ_S, and n_V with temperature of the steel in both heat treatment conditions are shown in **Figs.5.6, 5.7** and **5.8** respectively. Both the initial stress (σ_I) **(Fig.5.8)** and saturation stress (σ_S) **(Fig.5.9)** have increased on TMT and decreased continuously with temperature. Saturation stress (σ_S) is the stress at which work hardening rate ($\theta = d\sigma/d\varepsilon$) becomes zero at peak stress in the stress-strain curve. It is also a temperature dependent strength parameter and describes dynamic equilibrium between the strain hardening and recovery mechanisms. The decrease in σ_S with temperature implies that stress saturation with plastic deformation occurs at lower stress as recovery starts early with increase in temperature, signifying easy of dislocation movement with increase in temperature. The stress saturation with deformation, as interpreted by Mecking and Kocks, is controlled by the competition between production and annihilation (rearrangement) of dislocations until instability or necking sets-in the specimen during tensile deformation and the microstructure of the steel is expected to play a significant role in the work-hardening and recovery. Higher saturation stress on TMT means that the microstructural features makes the annihilation of dislocation more sluggish so that coupled with higher work-hardening capability **(Fig.5.8),** the saturation of stress occurs at high stress. True strain rate at saturated stress condition in tensile test and the steady state creep rate attained in the creep test are same as the similar underlying mechanisms resulting from the stationary state of dislocation substructures prevail [44]. Since the saturated stress is higher for the steel on TMT condition, the minimum/steady state creep rate of the TMT processed steel is expected to be less than that of the N+T steel, with increase in creep rupture strength.

The variation of Voce's recovery related parameter (n_V) with temperature for the RAFM steel in both N+T and AF-TMT25 conditions is shown in **Fig.5.7**. The absolute values of n_V is found to increase gradually with temperature in low and intermediate temperature regimes and beyond that they increased rapidly. In general, the absolute n_V values for AF-TMT25 condition are marginally lower than the N+T condition. The change in slope in the variation of n_V with temperature implies the change in deformation mechanism. It has been suggested that when cross slip dominates, the n_V is associated with relatively low value (absolute), whereas a change in controlling mechanism from cross-slip to climb and sub-boundary migration at higher temperatures resulted in very high n_V value. The temperature at which the change in slope occurs is found to increase on TMT. This indicates that the recovery of dislocations is delayed on TMT of the steel. Similar view has been expressed by **Vanaja et**

al. on the effect of tungsten on tensile flow behaviour. Tungsten increases the temperature at which change in slope of the variation of n_V with temperature occurs. The recovery is due to annihilation of excess dislocations by dislocation climb and the interaction of the dislocation with the carbides and other dislocations decreased the recovery process. TMT refines the martensitic lath structure with enhanced intragranular MX precipitation. Stable MX having small inter-particle spacing decreases the rate of recovery substantially on effecting pinning the dislocation and dictating link length of dislocation as the inter-particle spacing.

Applicability of Voce's constitutive equation has been judged on prediction of tensile strength and ductility. **Mishra et al.** have derived an expression, based on Voce's constitutive equation 5.5, to calculate ultimate tensile strength by invoking the Consideré criterion of instability at the onset of necking.

On differentiating equation 5.5 and substituting $\exp(n_v\varepsilon)$ with $(\sigma_S-\sigma)/(\sigma_S-\sigma_I)$, we get:

$$\frac{\partial\sigma}{\partial\varepsilon} = -n_V(\sigma_s-\sigma) \tag{5.6}$$

Now invoking Consideré criterion ($\partial\sigma/\partial\varepsilon=\sigma$) by substituting $\partial\sigma/\partial\varepsilon$ and σ with σ_{uv} (ultimate tensile strength estimated from Voce's constitutive equation), we have

$$\sigma_{uv} = n_V\sigma_s/(1-n_V) \tag{5.7}$$

The estimated ultimate tensile strength form Voce's constitutive equation (σ_{uv}) is plotted against experimental ultimate tensile strength in **Fig.5.8**. For the steel in both heat treated conditions, excellent correlation has been obtained between the estimated and experimental ultimate tensile strength.

The Voce's constitutive parameter σ_I, is the stress at the start of the plastic strain and so it can be correlated with the yield stress of the material. **Figure 5.9** compares the initial stress σ_i with the yield stress of the steel in both heat treated condition. Excellent agreement has been found.

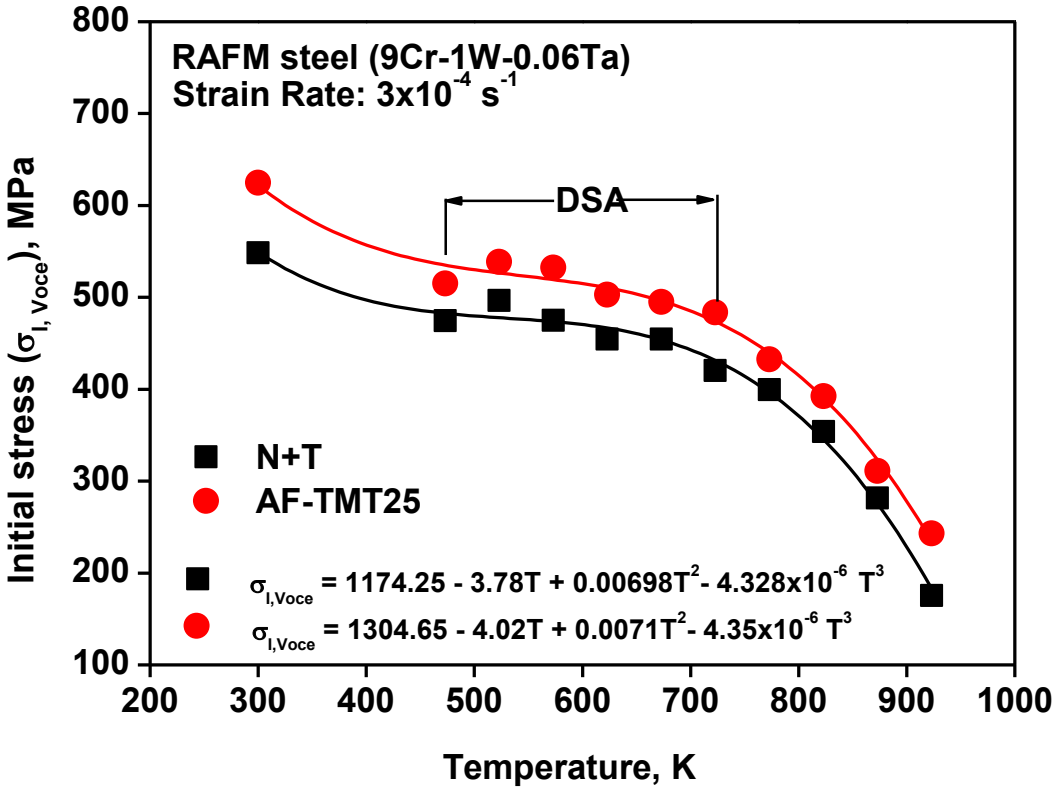

Fig.5.6. Temperature dependence of Voce's initial stress ($\sigma_{I,\,Voce}$) for RAFM steel in N+T and AF-TMT25 conditions.

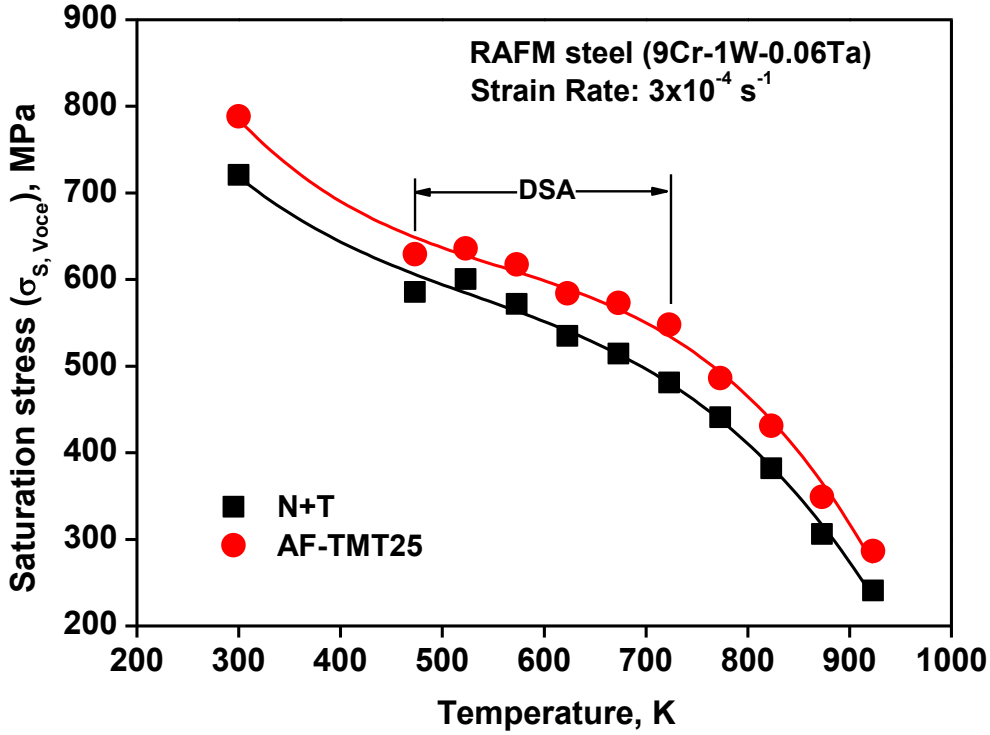

Fig.5.7. Temperature dependence of Voce's saturation stress ($\sigma_{S,\,Voce}$) for RAFM steel in N+T and AF-TMT25 conditions.

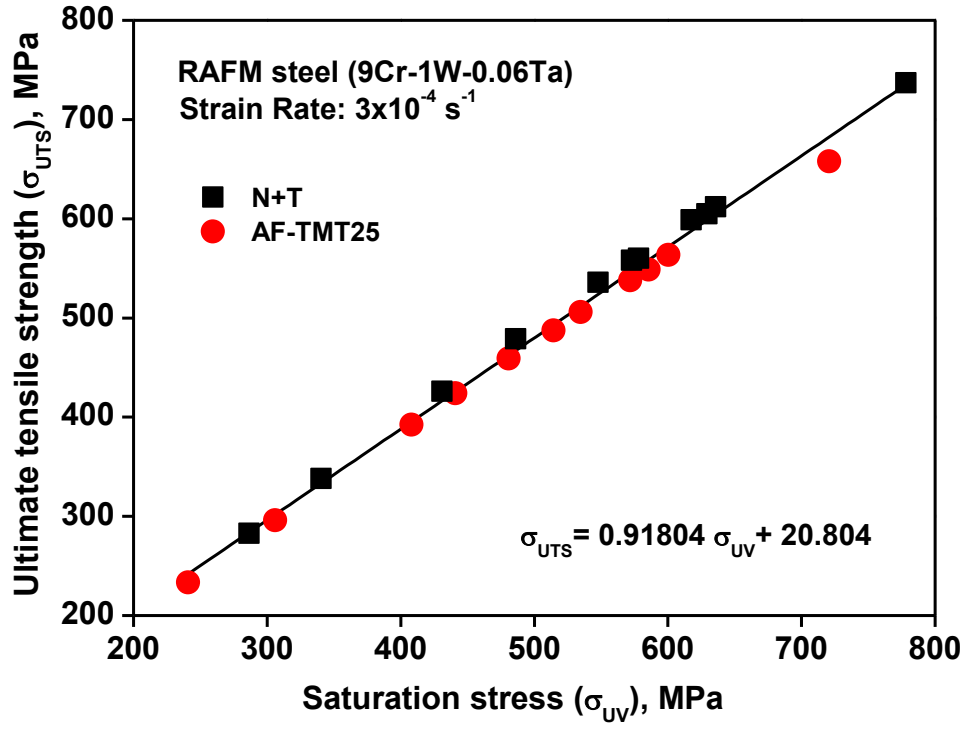

Fig.5.8. Comparison of ultimate tensile strength (σ_{UTS}) with Voce saturation stress (σ_{UV}) for RAFM steel in N+T and AF-TMT25 conditions.

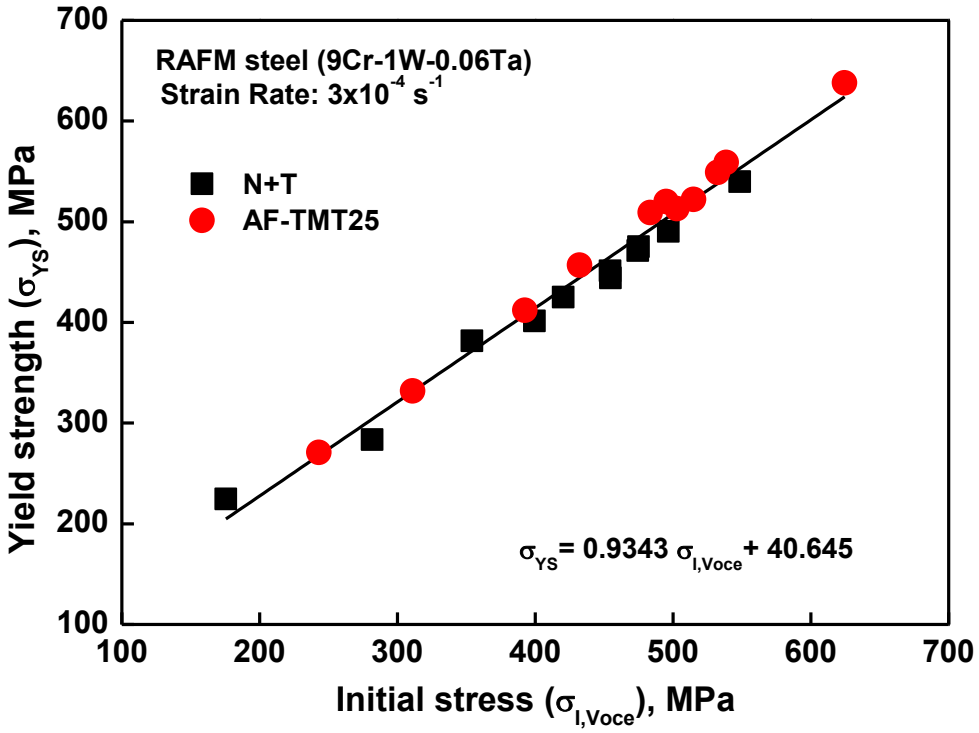

Fig.5.9. Comparison of true yield stress (σ_{YS}) with Voce initial stress ($\sigma_{I,\,Voce}$) for RAFM steel in N+T and AF-TMT25 conditions.

CONCLUSIONS

The following conclusions were drawn:

- TMT of the steel refined the microstructure of the tempered martensite having finer lath size with substantial fine precipitates.
- TMT of the steel increased the hardness and tensile strength coupled with increase in ductility and work-hardening rate.
- The tensile flow behaviour of the RAFM steel in all three conditions was adequately described by Voce's equation.
- TMT enhanced the tensile strength properties of RAFM steel without loss of ductility and is attributed to the refinement in microstructural features (lath width, precipitate size and distribution) of RAFM steel upon TMT.
- The steel in AF-TMT25 condition exhibited higher YS and UTS than the steel in the remaining two conditions. However, the YS and UTS of steel in FF-TMT25 condition are marginally higher than the steel in N+T condition.
- The steel in AF-TMT25 condition exhibited a higher % elongation than the steel in N+T. The % reduction in area varied in the order: N+T > AF-TMT25.
- The steel in N+T and AF-TMT25 conditions is found to undergo more thermal recovery at high temperatures (above 723 K) compared to FF-TMT25 condition.
- The tensile flow behaviour of RAFM steel in all three conditions was well described by Voce's equation. Experimental YS and UTS varied linearly with initial stress (σ_I) and saturation stress (σ_S) respectively, with $R^2 \geq 0.962$, irrespective of the TMT in different phase fields.
- Recovery behaviour of the steel as assessed by tempering response, stress relaxation and creep deformation behaviour is found more sluggish on imparting the steel with TMT.
- The most significant effect of TMT is the improvement in strength properties without loss of ductility, particularly in the case of AF-TMT25 condition of the RAFM steel.

REFERENCES

[1] R. L. Klueh and D. R. Harries, High-Chromium Ferritic and Martensitic Steels for Nuclear Applications, ASTM Monograph, ASTM International: West Conshohocken, (2001). https://doi.org/10.1520/MONO3-EB.

[2] A. Kohyama, Y. Kohno, K. Asakura, R&D of low activation ferritic steels for fusion in japanese universities, J. Nucl. Mater. 212–215 (1994) 684–89.

[3] N. Baluc, D.S. Gelles, S. Jitsukawa, A. Kimura, R.L. Klueh, G.R. Odette, B. van der Schaaf, J. Yu, Status of reduced activation ferritic/martensitic steel development, J. Nucl. Mater. 367-370 A (2007) 33–41. https://doi.org/10.1016/j.jnucmat.2007.03.036.

[4] S.N. Rosenwasser, P. Miller, J.A. Dalessandro, J.M. Rawls, W.E. Toffolo, W. Chen, The application of martensitic stainless steels in long lifetime fusion first wall/blankets, J. Nucl. Mater. 85–86 (1979) 177–182. https://doi.org/10.1016/0022-3115(79)90487-2.

[5] D.R. Harries, Ferritic Steels for Use in Nuclear Energy Technologies, in: J.W. Davis, and D.J. Michel (Eds.), Proc. Top. Conf., The Metallurgical Society of AIME, 1984: p. 141.

[6] K. Ehrlich, Materials research towards a fusion reactor, Fusion Eng. Des. 56–57 (2001) 71–82. https://doi.org/10.1016/S0920-3796(01)00236-8.

[7] R. W. Conn, Report of the DOE panel on low activation materials for fusion applications (UCLA/PPG-728), USA, 1983.

[8] T. Muroga, M. Gasparotto, S.J. Zinkle, Over view of materials research for fusion reactors, 62 (2008) 13–25.

[9] K. Ehrlich, S. Kelzenberg, H.D. Röhrig, L. Schäfer, M. Schirra, The development of ferritic-martensitic steels with reduced long-term activation, J. Nucl. Mater. 212–215 (1994) 678–683. https://doi.org/10.1016/0022-3115(94)90144-9.

[10] G.J. Butterworth, O.N. Jarvis, Comparison of transmutation and activation effects in five ferritic alloys and aisi 316 stainless steel in a fusion neutron spectrum, J. Nucl. Mater. 123 (1984) 982–988. https://doi.org/10.1016/0022-3115(84)90205-8.

[11] R.L. Klueh, E.E. Bloom, The development of ferritic steels for fast induced-radioactivity decay for fusion reactor applications, Nucl. Eng. Des. Fusion. 2 (1985) 383–389.
https://doi.org/10.1016/0167-899X(85)90026-6.

[12] D. Dulieu, K.W. Tupholme, G.J. Butterworth, Development of low-activation martensitic stainless steels, J. Nucl. Mater. 141–143 (1986) 1097–1101. https://doi.org/10.1016/0022-3115(86)90148-0.

[13] M. Tamura, H. Hayakawa, M. Tanimura, A. Hishinuma, T. Kondo, Development of potential low activation ferritic and austenitic steels, J. Nucl. Mater. 141–143 (1986) 1067–1073. https://doi.org/10.1016/0022-3115(86)90144-3.

[14] T. Noda, F. Abe, H. Araki, M. Okada, Development of low activation Ferritic steels, J. Nucl. Mater. 141–143 (1986) 1102–1106. https://doi.org/10.1016/0022-3115(86)90149-2.

[15] D. S. Gelles, Optimizing Materials for Nuclear Applications, in: Proc. Top. Conf., The Metallurgical Society of AIME, Warrendale, 1985: p. 63.

[16] Chen-YihHsuThomas A.Lechtenberg, Microstructure and mechanical properties of unirradiated low activation Ferritic steel, J. Nucl. Mater. 141–143 (1986) 1107–1112.

[17] D. Gelles, Effects of Irradiation on Low Activation Ferritic Alloys: A Review, in Reduced Activation Materials for Fusion Reactors, ed. R. Klueh, D. Gelles, M. Okada, and N. Packan (West Conshohocken, PA: ASTM International, 1990), 113-129.
https://doi.org/10.1520/STP24953S.

[18] R.L. Klueh, P.J. Maziasz, The microstructure of chromium-tungsten steels, Metall. Trans. A. 20 (1989) 373–382. https://doi.org/10.1007/BF02653916.

[19] H. Kayano, H. Kurishita, A. Kimura, M. Narui, M. Yamazaki, Y. Suzuki, Charpy impact testing using miniature specimens and its application to the study of irradiation behaviour of low-activation ferritic steels, J. Nucl. Mater. 179–181 (1991) 425–428. https://doi.org/10.1016/0022-3115(91)90115-N.

[20] G.J. Butterworth, L. Giancarli, Some radiological limitations on the compositions of low-activation materials for power reactors, J. Nucl. Mater. 155–157 (1988) 575–580. https://doi.org/10.1016/0022-3115(88)90374-1.

[21] G.J. Butterworth, Objectives and prospects for low-activation materials, J. Nucl. Mater. 179–181 (1991) 135–142. https://doi.org/10.1016/0022-3115(91)90028-6.

[22] F. Abe, M. Taneike, K. Sawada, Alloy design of creep resistant 9Cr steel using a dispersion of nano-sized carbonitrides, Int. J. Press. Vessel. Pip. 84 (2007) 3–12. https://doi.org/10.1016/j.ijpvp.2006.09.003.

[23] R.L. Klueh, D.J. Alexander, M.A. Sokolov, Effect of chromium , tungsten , tantalum , and boron on mechanical properties of 5–9Cr–WVTaB steels, J. Nucl. Mater. 304 (2002) 139–152. https://doi.org/10.1016/S0022-3115(02)00885-1

[24] L. Tan, Y. Yang, J.T. Busby, Effects of alloying elements and thermomechanical treatment on 9Cr Reduced Activation Ferritic – Martensitic (RAFM) steels, 442 (2013) 13–17.

[25] S. Hollner, B. Fournier, J. Le Pendu, T. Cozzika, I. Tournié, J.C. Brachet, A. Pineau, High-temperature mechanical properties improvement on modified 9Cr-1Mo martensitic steel through thermomechanical treatments, J. Nucl. Mater. 405 (2010) 101–108.
https://doi.org/10.1016/j.jnucmat.2010.07.034.

[26] G. McCracken, and, P. Stott, Fusion The Energy of the Universe, Academic Press, 2012.

[27] K. Shiba, M. Enoeda, S. Jitsukawa, Reduced activation martensitic steels as a structural material for ITER test blanket, J. Nucl. Mater. 329–333 (2004) 243–247. https://doi.org/10.1016/j.jnucmat.2004.04.018.

[28] P. Chakraborty, V. Kain, R. Tewari, G.K. Dey, Corrosion of an India produced RAFM steel in flowing lead-lithium eutectic, Fusion Eng. Des. 125 (2017) 269-276. https://doi.org/10.1016/j.fusengdes.2017.08.010.

[29] R.L. Klueh, Reduced-activation bainitic and martensitic steels for nuclear fusion applications, Curr. Opin. Solid State Mater. Sci. 8 (2004) 239–250. https://doi.org/10.1016/j.cossms.2004.09.004.

[30] C.P.C. Wong, J.F. Salavy, Y. Kim, I. Kirillov, E. Rajendra Kumar, N.B. Morley, S. Tanaka, Y.C. Wu, Overview of liquid metal TBM concepts and programs, Fusion Eng. Des. 83 (2008) 850–857. https://doi.org/10.1016/j.fusengdes.2008.06.040.

[31] K.L. Murty, I. Charit, Structural materials for Gen-IV nuclear reactors: Challenges and opportunities, J. Nucl. Mater. 383 (2008) 189–195. https://doi.org/10.1016/j.jnucmat.2008.08.044.

[32] E. Wakai, S. Jitsukawa, H. Tomita, K. Furuya, M. Sato, K. Oka, T. Tanaka, F. Takada, T. Yamamoto, Y. Kato, Y. Tayama, K. Shiba, S. Ohnuki, Radiation hardening and -embrittlement due to He production in F82H steel irradiated at 250°C in JMTR, J. Nucl. Mater. 343 (2005) 285–296. https://doi.org/10.1016/j.jnucmat.2004.10.167.

[33] R.L. Klueh, N. Hashimoto, M.A. Sokolov, P.J. Maziasz, K. Shiba, S. Jitsukawa, Mechanical properties of neutron-irradiated nickel-containing martensitic steels: II. Review and analysis of helium-effects studies, J. Nucl. Mater. 357 (2006) 169–182. https://doi.org/10.1016/j.jnucmat.2006.05.049.

[34] R. Lindau, A. Möslang, M. Rieth, M. Klimiankou, E. Materna-Morris, A. Alamo, A.A.F. Tavassoli, C. Cayron, A.M. Lancha, P. Fernandez, N. Baluc, R. Schäublin, E. Diegele, G. Filacchioni, J.W. Rensman, B. V.D. Schaaf, E. Lucon, W. Dietz, Present development status of EUROFER and ODS-EUROFER for application in blanket concepts, Fusion Eng. Des. 75–79 (2005) 989–996. https://doi.org/10.1016/j.fusengdes.2005.06.186.

[35] U. Fischer, S.P. Simakov, P.P.H. Wilson, Transmutation behaviour of Eurofer under irradiation in the IFMIF test facility and fusion power reactors, J. Nucl. Mater. 329–333 (2004) 228–232. https://doi.org/10.1016/j.jnucmat.2004.04.028.

[36] H. Nakamura, M. Ida, T. Chida, K. Shiba, K. Shimizu, M. Sugimoto, Thermo-structural analysis and design consideration of the replaceable backwall in IFMIF liquid lithium target, J. Nucl. Mater. 367-370 B (2007) 1543–1548. https://doi.org/10.1016/j.jnucmat.2007.04.021.

[37] A.K. Suri, N. Krishnamurthy, I.S. Batra, Materials issues in fusion reactors, J. Phys. Conf. Ser. 208 (2010). https://doi.org/10.1088/1742-6596/208/1/012001.

[38] Y. Kohno, A. Kohyama, T. Hirose, M.L. Hamilton, M. Narui, Mechanical property changes of low activation ferritic/ martensitic steels after neutron irradiation, J. Nucl. Mater. 271–272 (1999) 145–150. https://doi.org/10.1016/S0022-3115(98)00735-1.

[39] G. Aiello, J. Aktaa, F. Cismondi, G. Rampal, J.F. Salavy, F. Tavassoli, Assessment of design limits and criteria requirements for Eurofer structures in TBM components, J. Nucl. Mater. 414 (2011) 53–68. https://doi.org/10.1016/j.jnucmat.2011.05.005.

[40] R.L. Klueh, Elevated temperature ferritic and martensitic steels and their application to future nuclear reactors, Int. Mater. Rev. 50 (2005) 287–310. https://doi.org/10.1179/174328005X41140.

[41] F. Abe, T. Horiuchi, M. Taneike, K. Sawada, Stabilization of martensitic microstructure in advanced 9Cr steel during creep at high temperature, Mater. Sci. Eng. A. 378 (2004) 299–303. https://doi.org/10.1016/j.msea.2003.11.073.

[42] F. Abe, Precipitate design for creep strengthening of 9% Cr tempered martensitic steel for ultra-supercritical power plants, Sci. Technol. Adv. Mater. 9 (2008). https://doi.org/10.1088/1468-6996/9/1/013002.

[43] R.L. Klueh, N. Hashimoto, P.J. Maziasz, Development of new ferritic/martensitic steels for fusion applications, Proc. - Symp. Fusion Eng. 00 (2006) 1–4. https://doi.org/10.1109/FUSION.2005.252908.

[44] J. Vanaja, K. Laha, M.D. Mathew, T. Jayakumar, E. Rajendra Kumar, Effects of tungsten and tantalum on creep deformation and rupture properties of Reduced Activation Ferritic-Martensitic steel, Procedia Eng. 55 (2013) 271–276. https://doi.org/10.1016/j.proeng.2013.03.253.

[45] R.L. Klueh, Elevated temperature ferritic and martensitic steels and their application to future nuclear reactors. Int. Mater. Rev., 50 (5), (2005) 287–310. https://doi.org/10.2172/885938.

[46] T. Jayakumar, M.D. Mathew, K. Laha, R. Sandhya, Materials development for fast reactor applications, Nucl. Eng. Des. 265 (2013) 1175–1180. https://doi.org/10.1016/j.nucengdes.2013.05.001.

[47] Y. Chen, K. Sridharan, S. Ukai, T.R. Allen, Oxidation of 9Cr oxide dispersion strengthened steel exposed in supercritical water, J. Nucl. Mater. 371 (2007) 118–128. https://doi.org/10.1016/j.jnucmat.2007.05.018.

[48] S. Ukai, T. Nishida, T. Okuda, T. Yoshitake, R&D of oxide dispersion strengthened ferritic martensitic steels for FBR, J. Nucl. Mater. 258–263 (1998) 1745–1749. https://doi.org/10.1016/S0022-3115(98)00241-4.

[49] K. Laha, S. Saroja, A. Moitra, R. Sandhya, M.D. Mathew, T. Jayakumar, E. Rajendra Kumar, Development of India-specific RAFM steel through optimization of tungsten and tantalum contents for better combination of impact, tensile, low cycle fatigue and creep properties, J. Nucl. Mater. 439 (2013) 41–50. https://doi.org/10.1016/j.jnucmat.2013.03.073.

[50] B. Raj, T. Jayakumar, Development of Reduced Activation Ferritic-Martensitic Steels and fabrication technologies for Indian test blanket module, J. Nucl. Mater. 417 (2011) 72–76. https://doi.org/10.1016/j.jnucmat.2011.02.032.

[51] R. Schaeublin, T. Leguey, P. Spätig, N. Baluc, M. Victoria, Microstructure and mechanical properties of two ODS ferritic/martensitic steels, J. Nucl. Mater. 307–311 (2002) 778–782. https://doi.org/10.1016/S0022-3115(02)01193-5.

[52] B. Raj, S.L. Mannan, P.R. Vasudeva Rao, M.D. Mathew, Development of fuels and structural materials for fast breeder reactors, Sadhana - Acad. Proc. Eng. Sci. 27 (2002) 527–558. https://doi.org/10.1007/BF02703293.

[53] E.E. Bloom, The challenge of developing structural materials for fusion power systems, J. Nucl. Mater. 258–263 (1998) 7–17. https://doi.org/10.1016/S0022-3115(98)00352-3.

[54] C.B.A. Forty, Activation Response of Martensitic Steels, J. Fusion Energy. 16 (1997) 277–283. https://doi.org/10.1023/A:1021859724086.

[55] E. Lucon, Mechanical tests on two batches of oxide dispersion strengthened RAFM steel (EUROFER97), Fusion Eng. Des. 61–62 (2002) 683–689. https://doi.org/10.1016/S0920-3796(02)00098-4.

[56] L. Huang, X. Hu, W. Yan, W. Sha, F. Xiao, Y. Shan, K. Yang, Laves-phase in the China Low Activation Martensitic steel after long-term creep exposure, Mater. Des. 63 (2014) 333–335. https://doi.org/10.1016/j.matdes.2014.06.028.

[57] R. Jayaram, R.L. Klueh, Microstructural characterization of 5 to 9 pct Cr-2 pct W-V-Ta martensitic steels, Metall. Mater. Trans. A, Phys. Metall. Mater. Sci. 29 (1998) 1551–1558. https://doi.org/10.1007/s11661-998-0077-2.

[58] F. Abe, T. Noda, M. Okada, Optimum alloy compositions in reduced-activation martensitic 9Cr steels for fusion reactor, J. Nucl. Mater. 195 (1992) 51–67. https://doi.org/10.1016/0022-3115(92)90363-P.

[59] Z.X. Xia, C. Zhang, H. Lan, Z.G. Yang, P.H. Wang, J.M. Chen, Z.Y. Xu, X.W. Li, S. Liu, Influence of smelting processes on precipitation behaviours and mechanical properties of low activation ferrite steels, Mater. Sci. Eng. A. 528 (2010) 657–662. https://doi.org/10.1016/j.msea.2010.09.088.

[60] Y. De Carlan, A. Alamo, M.H. Mathon, G. Geoffroy, A. Castaing, Effect of thermal aging on the microstructure and mechanical properties of 7-11 CrW steels, J. Nucl. Mater. 283–287 (2000) 672–676. https://doi.org/10.1016/S0022-3115(00)00277-4.

[61] A. Danón, A. Alamo, Behaviour of Eurofer97 reduced activation martensitic steel upon heating and continuous cooling, J. Nucl. Mater. 307–311 (2002) 479–483. https://doi.org/10.1016/S0022-3115(02)01209-6.

[62] R.R.L. M. Gasparotto, Proceedings of the Int. Conf. Nuclear Energy for. New Europe, Slovenia, in: R.R.L. M. Gasparotto (Ed.), Slovenia, n.d.

[63] L. Schäfer, M. Schirra, Influence of thermal aging on tensile and impact bending properties of the steel grades OPTIFER and F82H mod, J. Nucl. Mater. 271–272 (1999) 455–458. https://doi.org/10.1016/S0022-3115(98)00757-0.

[64] P. H. Wang, J.M.Chen, Z.Y.Xu, S. Liu, X.W. Li, and H.Y. Fu., Research and development of reduced activation ferritic/martensitic steel CLF-1 at SWIP, in: IAEA Fusion Energy Conf., IAEA, Daejon, Korea (2010).

[65] Harrelson, K.J., S.H. Rou, and R.C. Wilcox, Impurity element effects on the toughness of 9Cr-1Mo steel, J. Nucl. Mater. 141–143 (1986) 508–512.

[66] P. Hofer, M.K. Miller, S.S. Babu, S.A. David, H. Cerjak, Investigation of boron distribution in martensitic 9% Cr creep resistant steel, ISIJ Int. 42 (2002) 62–66. https://doi.org/10.2355/isijinternational.42.suppl_s62.

[67] H.K. Danielsen, J. Hald, Behaviour of z phase in 9–12%Cr steels, Energy Mater. Mater. Sci. Eng. Energy Syst. 1 (2006) 49–57. https://doi.org/10.1179/174892306X99732.